Journal of Energy Chemistry 67 (2022) 432–450

Contents lists available at ScienceDirect

Journal of Energy Chemistry

journal homepage: www.elsevier.com/locate/jechem

http://www.journals.elsevier.com/journal-of-energy-chemistry/

Recent advances in electrocatalytic oxygen reduction for on-site hydrogen peroxide synthesis in acidic media

Jun-Yu Zhang [a], Chuan Xia [b,c], Hao-Fan Wang [d], Cheng Tang [a,*]

[a] School of Chemical Engineering and Advanced Materials, The University of Adelaide, Adelaide, SA 5005, Australia
[b] Yangtze Delta Region Institute (Huzhou), University of Electronic Science and Technology of China, Huzhou 313001, Zhejiang, China
[c] School of Materials and Energy, University of Electronic Science and Technology of China, Chengdu 611731, Sichuan, China
[d] AIST-Kyoto University Chemical Energy Materials Open Innovation Laboratory (ChEM-OIL), National Institute of Advanced Industrial Science and Technology (AIST), Sakyo-ku, Kyoto 606-8501, Japan

ARTICLE INFO

Article history:
Received 30 September 2021
Revised 13 October 2021
Accepted 13 October 2021
Available online 27 October 2021

Keywords:
Hydrogen peroxide
Oxygen reduction reaction
Acidic media
Selectivity
Electrosynthesis

ABSTRACT

Electrocatalytic oxygen reduction reaction (ORR) via two-electron pathway is a promising approach to decentralized and on-site hydrogen peroxide (H_2O_2) production beyond the traditional anthraquinone process. In recent years, electrochemical H_2O_2 production in acidic media has attracted increasing attention owing to its stronger oxidizing capacity, superior stability, and higher compatibility with various applications. Here, recent advances of H_2O_2 electrosynthesis in acidic media are summarized. Specifically, fundamental aspects of two-electron ORR mechanism are firstly presented with an emphasis on the pH effect on catalytic performance. Major categories of promising electrocatalysts are then reviewed, including noble-metal-based materials, non-noble-metal single-atom catalysts, non-noble-metal compounds, and metal-free carbon-based materials. The innovative development of electrochemical devices and *in situ*/on-site application of electrogenerated H_2O_2 are also highlighted to bridge the gap between laboratory-scale fundamental research and practically relevant H_2O_2 electrosynthesis. Finally, critical perspectives on present challenges and promising opportunities for future research are provided.

Jun-Yu Zhang received his B.E. degree from the School of Environment, Tsinghua University in 2018, and M.S. degree from the Department of Civil and Environmental Engineering, Stanford University in 2020. He is currently pursuing his Ph.D. degree in the School of Chemical Engineering and Advanced Materials, The University of Adelaide. His research focuses on developing nanomaterials for electrocatalytic sustainable production of fuels and chemicals.

Chuan Xia is currently a Professor at the School of Materials and Energy of The University of Electronic Science and Technology of China (UESTC), China. Dr. Xia received his Ph.D. in materials science and engineering from the King Abdullah University of Science and Technology (KAUST) in 2018 followed by a postdoctoral training at Harvard university and Rice university. He focus on developing methods for controlling the architecture of molecules and materials, understanding their fundamental properties, and utilizing such structures to develop novel catalysts that can be applied in the areas of electrocatalysis, energy generation, storage, and conversion. He was recently honored with the J. Evans Attwell-Welch postdoctoral fellowship award (2019) and the best applied paper award of AIChE STS (2020).

* Corresponding author.
E-mail address: cheng.tang@adelaide.edu.au (C. Tang).

https://doi.org/10.1016/j.jechem.2021.10.013

Hao-Fan Wang received his B.E. and Ph.D. degrees from the Department of Chemical Engineering, Tsinghua University in 2013 and 2018, respectively. Then he works at AIST-Kyoto University Chemical Energy Materials Open Innovation Laboratory (ChEM-OIL) as a postdoctoral researcher. His research interests include carbon materials, MOF-derived materials, and their applications in electrocatalysis and metal–air batteries.

Cheng Tang received his B.E. and Ph.D. degrees from the Department of Chemical Engineering, Tsinghua University in 2013 and 2018, respectively. Currently, he is a Lecturer at The University of Adelaide after three-year postdoctoral research there. His research focuses on the atomic-level design and mechanism understanding of advanced nanomaterials for high-performance batteries and electrochemical production of fuels and chemicals. He was recently honored with the ARC Discovery Early Career Researcher Award (2022), the MIT Technology Review Innovators Under 35 Asia Pacific (2021), the Thomson Reuters/Clarivate Analytics Highly Cited Researcher (2020), and The Chorafas Foundation Award in Chemistry (2019).

1. Introduction

Hydrogen peroxide (H_2O_2) is recognized as one of the 100 most important chemicals in the world with its annual production reaching 5.5 million tons in 2015 [1,2]. As a versatile and green oxidant, H_2O_2 is widely used in pulp and textile bleaching, chemical synthesis, disinfection and wastewater treatment [3–7]. Remarkably, U.S. Environmental Protection Agency listed H_2O_2 as one important disinfectant for COVID-19 [8], which has also been proposed to play a pivotal role in reducing the hospitalization rate and complications with the use of 0.5–3 wt% H_2O_2 [9]. Currently, more than 95% of H_2O_2 are synthesized by the multi-step anthraquinone process [10]. However, this process requires huge and centralized infrastructure, which makes it unsuitable for on-site and on-demand H_2O_2 production in remote areas. To lower the transportation and storage costs, additional distillation processes are performed to generate up to 70 wt% H_2O_2, leading to significant safety hazards. Other drawbacks of anthraquinone process include the substantial volume of waste generated from organic solvents, and extra costs incurred by the removal of unwanted stabilizers. To achieve decentralized H_2O_2 production, a more straightforward route is the direct synthesis of H_2O_2 from hydrogen (H_2) and oxygen (O_2) over Pd-based catalysts [11–14]. However, the mixture of H_2 and O_2 is explosive and thus requires dilution to keep away from the flammable range, which significantly limits the efficiency of this process. In addition, similar to anthraquinone process, direct synthesis also involves undesired removal of toxic additives such as acid promoters and halide ions. Consequently, there has been increasing interest in finding alternative methods that can overcome the issues related to anthraquinone and direct synthesis processes.

Compared with above-mentioned methods, electrocatalytic oxygen reduction reaction (ORR) under ambient conditions offers a safe and environmentally friendly solution to decentralized H_2O_2 synthesis [15–19]. In ORR, oxygen molecules can be reduced to H_2O via four-electron ($4e^-$) reaction pathway or H_2O_2 via two-electron ($2e^-$) pathway [20]. Traditionally, $4e^-$ ORR is the cathode reaction in fuel cells, but if the selectivity is steered toward $2e^-$ process, *in situ* H_2O_2 production can be achieved in fuel cell configurations while generating electric energy, and the danger of explosion is avoided by separating H_2 and O_2 [21]. H_2O_2 can also be formed in electrolysis cells powered by renewable electricity, which is an intrinsically green process and could be easily controlled by the applied potential. For electrochemical H_2O_2 production, the pH value of electrolyte is a critical parameter. While $2e^-$ ORR could occur in acidic, neutral or basic electrolytes, producing H_2O_2 in acidic environment is particularly attractive for a number of reasons. Firstly, given the acid dissociation constant of H_2O_2 (pK_a = 11.7), its main form in acidic media would be H_2O_2 instead of HO_2^-. The stronger oxidation capacity of acidic H_2O_2 enables its efficient utilization in various industrial processes [22]. Secondly, H_2O_2 is more stable in acidic than in alkaline environment, as higher pH would facilitate its decomposition [23]. Thirdly, acidic H_2O_2 production is attainable in proton exchange membrane (PEM)-type devices, and PEM is a mature technology with good stability and ionic conductivity. Since H_2O_2 is the thermodynamically unfavorable product of ORR [24], rational design of electrocatalysts with high activity, selectivity and stability toward $2e^-$ ORR pathway is a precondition for acidic H_2O_2 generation.

To date, numerous materials have been identified as promising $2e^-$ ORR electrocatalysts in acidic electrolyte [6], such as noble metals and their alloys, non-noble transition metal compounds, single-atom catalysts (SACs), and metal-free carbon-based materials. Noble metal-based materials are currently the state-of-the-art catalysts in acidic media with outstanding ORR activity and H_2O_2 selectivity. However, their scarcity and high cost largely hinder the practical application and trigger research in non-noble metal catalysts as promising alternatives. The performance of non-noble metal catalysts is generally inferior in acidic media to that in alkaline media. Catalyst engineering and a thorough understanding of pH effect are thus imperative to improve their catalytic performance [25]. Furthermore, beyond the development of electrocatalysts, innovations in electrochemical devices that scale up laboratory tests to practical applications are also necessary. In the 1930s, Berl pioneered the development of electrocatalytic ORR for H_2O_2 production [26]. This process was later commercialized to produce dilute H_2O_2 solution in alkaline media and used for pulp and paper bleaching, known as Huron-Dow process [14]. However, compared with catalyst design, relatively fewer efforts have been devoted to reactor design beyond such traditional processes for a long time. Recent progress in electrocatalysts has inspired a variety of novel device configurations to produce bulk or even pure H_2O_2 solution, such as flow cell, phase-transfer device, and solid electrolyte cell [27,28]. The electrogenerated H_2O_2 in devices has shown promise for *in situ* applications in degradation of organic pollutants, disinfection and chemical synthesis [29–31]. Ultimately, the combined progress of mechanistic insights, catalyst design, and electrochemical cell design will help realize practical H_2O_2 electrosynthesis and utilization.

Considering these facts, this review aims to sum up recent advances of H_2O_2 production from ORR in acidic environment. Firstly, fundamental aspects of acidic $2e^-$ ORR will be provided, with special emphasis placed on the reaction mechanism and the influence of electrolyte pH on catalytic performance over metal and non-metal catalysts. Based on this mechanistic understanding, major categories of state-of-the-art electrocatalysts and their design strategies toward acidic H_2O_2 production will be summarized, including noble-metal based nanoparticles and SACs, non-noble-metal SACs, non-noble-metal compounds and metal-free carbon-based materials. Furthermore, the practical electrochemical devices for H_2O_2 generation and the *in situ* applications of electrogenerated H_2O_2 will be discussed in detail. In the final section,

the critical challenges, future opportunities and research directions in the field of acidic 2e⁻ ORR will be presented.

2. Fundamental aspects of acidic H_2O_2 production from ORR

2.1. Reaction mechanism

In general, electrocatalytic oxygen reduction is a multi-step reaction that can proceed through the competing 4e⁻ and 2e⁻ reaction pathways (Fig. 1a) [20]. In acidic media, the 4e⁻ pathway generates water (H_2O) as the final product ($O_2 + 4H^+ + 4e^- \rightarrow 2H_2O$, E^o = 1.23 V vs reversible hydrogen electrode (RHE)) and involves three intermediates (*OOH, *O and *OH), which is extensively studied for fuel cell and metal–air battery applications [32,33]. On the other hand, the 2e⁻ pathway leads to H_2O_2 generation ($O_2 + 2H^+ + 2e^- \rightarrow H_2O_2$, E^o = 0.70 V vs RHE). The 2e⁻ pathway is comprised of two proton-coupled electron transfer (PCET) steps with only *OOH intermediate, as shown in Eqs. (1) and (2):

$$O_2 + * + (H^+ + e^-) \rightarrow *OOH \quad (1)$$

$$*OOH + (H^+ + e^-) \rightarrow H_2O_2 + * \quad (2)$$

For selective 2e⁻ ORR to happen, the cleavage of O–O bond should be avoided in order to suppress the undesirable formation of water. Both pathways share the common *OOH intermediate. The binding free energy of *OOH intermediate on the electrocatalyst (ΔG_{*OOH}) should be appropriate, such that the O–O bond is preserved during catalysis [20]. Ideally, the binding strength of oxygen molecules on catalyst surface should be strong enough to facilitate the production of *OOH, meanwhile the *OOH adsorption should be weak enough to allow H_2O_2 desorption. Therefore, an optimal catalyst needs to overcome the kinetic barriers of O_2 activation and *OOH protonation (desorption) for high activity, while maximize the kinetic barrier of *OOH dissociation (reduction) for high selectivity [34,35].

During ORR process, the adsorption of oxygen molecule is the first step and can provide unique insights into selectivity. The oxygen molecule can adsorb on the metal surface by three different modes: Pauling-type (end-on adsorption on one surface atom), Griffith-type (side-on adsorption on one surface atom) and Yeager-type (side-on adsorption on two surface atoms) (Fig. 1b) [3,22,36,37]. The adsorption mode of oxygen is an important determinant of ORR selectivity. On bulk metal surfaces, side-on adsorption can elongate and weaken the O–O bond while the resulting *O and *OH intermediates can adsorb onto adjacent atoms, leading to significant H_2O production. In contrast, SACs with isolated active centers would favor end-on adsorption, which lowers the possibility of O–O bond cleavage with inherent advantage for H_2O_2 production [21,38,39]. Thus, optimizing the adsorption strength of reaction intermediates by tuning adsorption configurations represents a general strategy to design high-performance 2e⁻ ORR catalysts.

Over the past years, density functional theory (DFT) calculation has provided powerful tools for describing adsorption energies of intermediates on catalyst surface, and the results can be well-correlated with experiments in acidic media [21,40,41]. Nørskov

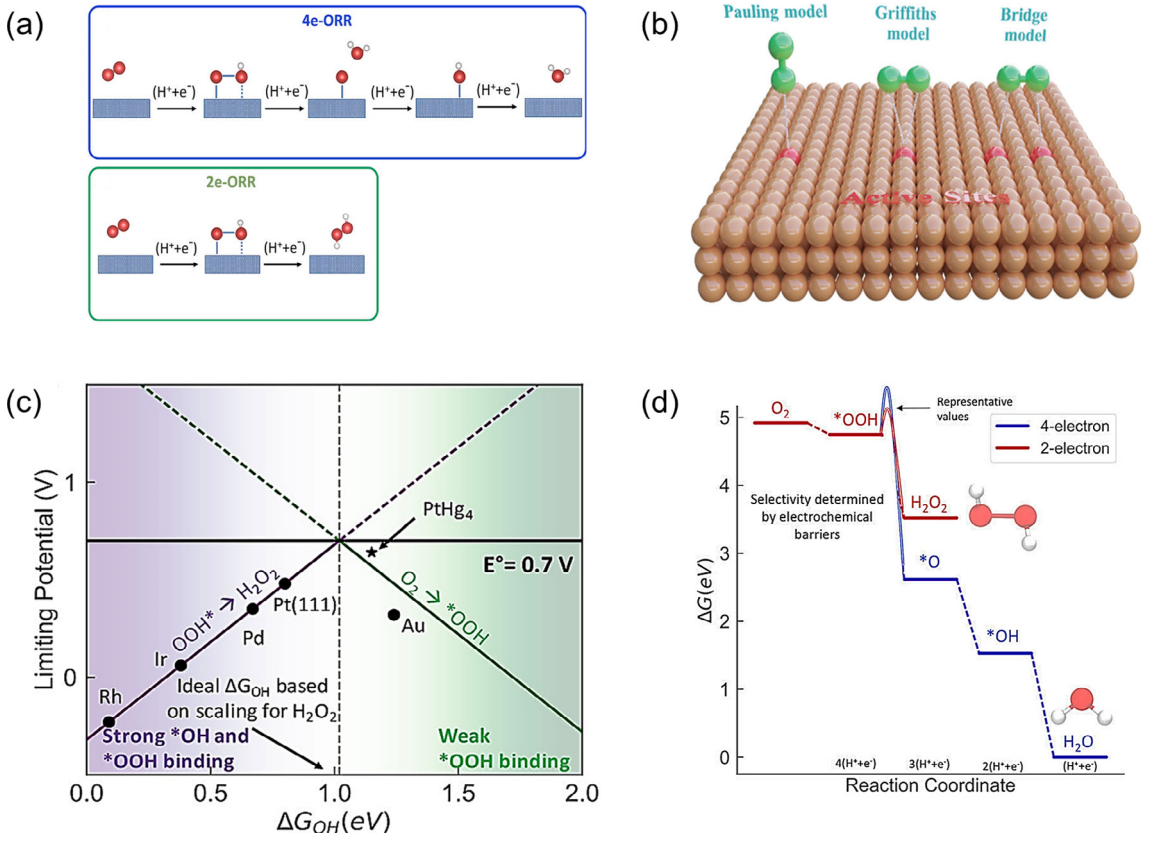

Fig. 1. Reaction mechanism of 2e⁻ ORR in acidic media. (a) Schematic illustration of 4e⁻ and 2e⁻ ORR pathways. Reprinted from Ref. [20] with permission from the American Chemical Society. (b) Schematic illustration of three adsorption modes of molecular oxygen on catalytic active sites. Reprinted from Ref. [36] with permission from the Royal Society of Chemistry. (c) Sabatier volcano plot of 2e⁻ ORR. (d) Free energy diagram of 4e⁻ and 2e⁻ ORR pathways on Au (111) surface. (c and d) are reprinted from Ref. [24] with permission from the American Chemical Society.

et al. developed a computational hydrogen electrode (CHE) model to calculate the adsorption free energy of intermediates in which the chemical potential of a proton-electron pair is equivalent to that of 1/2 H_2 in gas phase at an electrode potential of U = 0 V [42]. The influence of electrode potential on free energies of intermediates is considered by defining the free energy of a proton-electron pair as $-eU$, where e is elementary charge and U is electrode potential vs RHE. The scaling relation implies that there is only one degree of freedom in ORR [43], as the free energies of intermediates on metal surfaces are correlated by the equations: $\Delta G_{*OOH} = \Delta G_{*OH} + 3.2 \pm 0.2$ eV and $\Delta G_{*O} = 2\Delta G_{*OH}$. ΔG_{*OH} can be used as a descriptor to construct a volcano-type relationship, where the limiting potentials are plotted as a function of ΔG_{*OH} (Fig. 1c) [24,35]. The lower limiting potential lines (solid lines) comprise the limiting potential for the overall reaction, and their intersection at the peak of volcano plot corresponds to the equilibrium limiting potential of 2e⁻ ORR (0.70 V vs RHE). For catalysts at the left segment of the volcano, the strong binding of *OOH leads to easier formation of *O and *OH, causing the domination of 4e⁻ pathway. For catalysts lying on the right segment of the volcano, the weak binding of *OOH increases H_2O_2 selectivity but decreases ORR activity [44]. Based on the classic Sabatier principle, an ideal catalyst should be situated near the volcano peak to have moderate binding strength of ΔG_{*OH} and thus optimal H_2O_2 production. Besides, kinetic parameters are also important to complement thermodynamic analysis and rationalize experimentally observed selectivity (Fig. 1d) [24]. For example, in the case of Au (111) surface, the free energy diagram indicates that the step of *OOH to H_2O_2 is thermodynamically unfavorable as compared with O–O bond cleavage, but Au (111) is experimentally selective for H_2O_2 formation due to the lower kinetic barrier of H_2O_2 formation step [24,40]. This finding highlights the crucial roles of kinetic aspects in determining ORR selectivity. The combination of thermodynamic and kinetic insights will help guide rational design of electrocatalysts that are selective for H_2O_2 production with low overpotentials [34].

2.2. pH effect

Since the activity and selectivity of 2e⁻ ORR catalysts strongly depend on the pH values of electrolyte, it is critical to understand the effects of pH for rational catalyst design in acidic media. For example, the pH dependence for H_2O_2 production on extended surfaces of polycrystalline (pc) Pt, Pt-Hg, Ag, Ag-Hg and glassy carbon was studied in 0.1 M $HClO_4$ and 0.1 M KOH [14]. Ag(pc), Pt-Hg(pc) and Ag-Hg(pc) exhibited much higher selectivity toward H_2O_2 production but slightly lower ORR activity in acidic media relative to alkaline media (Fig. 2a) [14]. In contrast, glassy carbon exhibited similar selectivity regardless of electrolyte pH, but its ORR current density in 0.1 M $HClO_4$ was smaller than that in 0.1 M KOH. They reasoned that all catalysts studied bind *OOH weakly and their ORR activity would be limited by *OOH formation in acidic media.

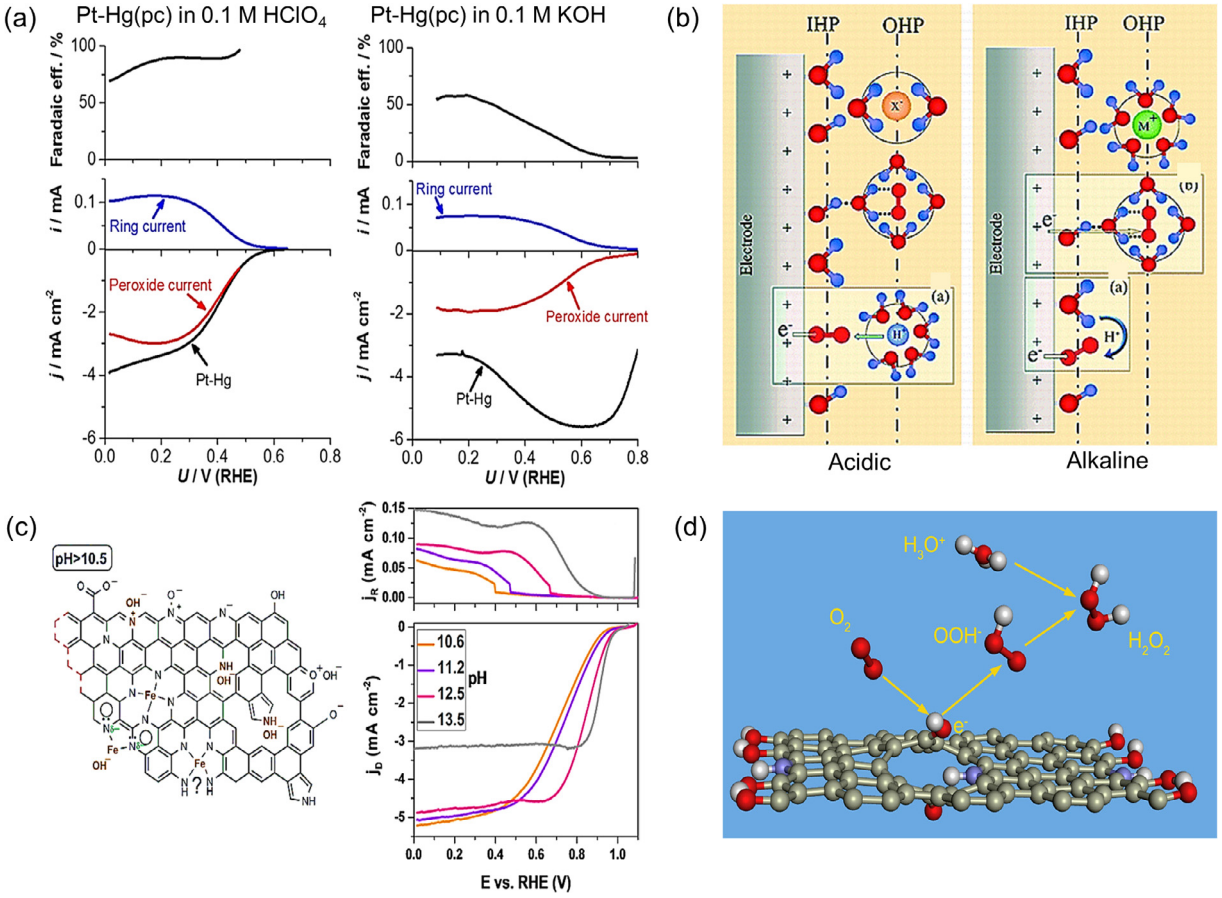

Fig. 2. The effect of pH on 2e⁻ ORR process. (a) RRDE measurements and Faradaic efficiencies of polycrystalline Pt-Hg in 0.1 M $HClO_4$ and 0.1 M KOH. Reprinted from Ref. [14] with permission from the American Chemical Society. (b) Schematic illustration of inner- and outer-sphere electron transfer ORR mechanisms in acidic (left) and alkaline (right) electrolytes, respectively. Red: oxygen; Blue: hydrogen; Green: Alkali metal cation; Orange: Supporting electrolyte anion. Reprinted from Ref. [45] with permission from the American Chemical Society. (c) Surface chemistry and RRDE measurements of Fe-N-C catalysts in electrolytes with pH > 10.5. Reprinted from Ref. [46] with permission from the American Chemical Society. (d) OOH^- ion mechanism of 2e⁻ ORR on carbon catalysts. Reprinted from Ref. [60] with permission from the American Chemical Society.

For metal-based catalysts, the kinetic barrier for O–O bond dissociation is higher in acidic media than that in alkaline media, indicating a less favored 4e⁻ ORR pathway and more selective H_2O_2 electrosynthesis in acidic media [14]. Compared to metal-based catalysts, the ORR activity of carbon-based catalysts is lower due to the intrinsically weaker *OOH binding, but their selectivity is less influenced by electrolyte pH.

The difference in electron transfer mechanisms under different pH conditions can also influence catalytic ORR performance. By varying electrolyte pH from 0 to 14, different species are present in the inner-Helmholtz plane (IHP) and outer-Helmholtz plane (OHP) of the double-layer structure at electrode-electrolyte interface (Fig. 2b) [45]. In acidic media, IHP consists of chemisorbed molecular O_2, adsorbed hydroxyl species (OH_{ads}) and solvent water dipoles, whereas OHP is populated by solvated molecular O_2 and electrolyte anions. As protons are abundant and highly mobile in acidic electrolyte, superoxide radical anion $(\cdot O_2^-)_{ads}$ species formed by the first electron transfer to the adsorbed O_2 would soon be protonated with $4H^+$ and 4e⁻ to form H_2O as the final product. Under this circumstance, 4e⁻ ORR is promoted by the predominant inner-sphere electron transfer mechanism, with directly adsorbed molecular O_2 onto pristine Pt surfaces and stabilization of peroxide intermediate [45]. On the other hand, in a highly alkaline environment, water is both the proton source and the solvent, and the low rate of proton transfer is conducive to $(\cdot O_2^-)_{ads}$ stabilization. In this case, outer-sphere electron transfer can occur by the non-covalent interaction (hydrogen bond) between *OH and the solvated $O_2\cdot(H_2O)_n$ cluster, which allows the desorption of *OOH intermediate and formation of HO_2^-. However, it is noticeable that the above explanation may not be applicable to some well-performed noble-metal catalysts in acidic media [7] and therefore more elaborate models are required to fully understand the pH-dependent 2e⁻ ORR behaviors.

The pH dependence of non-noble metal-nitrogen-carbon (M-N-C) catalysts in ORR have also been reported [46,47]. Researchers studied the surface chemistry of Fe-N-C catalyst over a wide pH range (1.1–13.5) using X-ray photoelectron spectroscopy (XPS) in order to unveil the relationship between electrolyte pH and ORR activity/selectivity (Fig. 2c) [46]. It was shown that the number of accessible Fe–N_x sites decreases with hydroxyl concentration. When the electrolyte pH is below 10.5, ORR is limited by PCET, and the protons on the surface of Fe-N-C catalyst neutralize adsorbed OH^- toward 4e⁻ ORR on Fe–N_x active sites. When pH value is higher than 10.5, the excess OH^- ions adsorbed at Fe–N_x centers make ORR occur via the OHP mechanism, which is favorable for H_2O_2 production via 2e⁻ ORR. Moreover, protonation of pyridinic nitrogen is critical to H_2O_2 production as it can provide protons for ORR and neutralize the adsorbed OH^- at Fe–N_x centers. Besides Fe-N-C, Co-N-C catalyst manifests pH-related ORR activity, selectivity and mechanism as well [47]. H_2O_2 selectivity of Co-N-C depends on both pH and potential; in acidic media, H_2O_2 selectivity increases with more negative potential, whereas in neutral and alkaline media, H_2O_2 selectivity remains nearly unchanged over the entire potential range.

The 2e⁻ ORR performance of carbon-based metal-free catalysts under varying pH conditions is remarkably different from that of metal-based catalysts. In general, many functionalized carbon materials, such as defective carbon [48–50], oxidized carbon materials [51,52], nitrogen-doped carbons [53–55], boron-doped carbons [56], and boron-nitrogen co-doped carbon [57], can perfectly catalyze 2e⁻ ORR in alkaline media with a low overpotential and outstanding H_2O_2 selectivity (> 90%). In neutral and acidic media, some carbon catalysts still maintain high selectivity, but their overpotentials are usually high due to the intrinsically weak *OOH adsorption [14]. In one study of N-doped carbon materials, the best H_2O_2 selectivity and durability were achieved in neutral solution, where independent rotating ring disk electrode (RRDE) and photometric UV–Vis techniques showed that H_2O_2 selectivity and formation rates are strongly dependent on pH in the order of neutral ($KClO_4$) > acid ($HClO_4$) >-alkaline (KOH) on mesoporous N-doped carbons [58]. However, the reaction mechanism for neutral H_2O_2 synthesis is unclear and highly efficient catalysts are rather rare. Noffke et al. proposed an interface solvation model to understand acidic and alkaline ORR selectivity of a N-doped graphene nanostructure [59]. As in enzyme-catalyzed reactions, the hydrophobic microenvironment around carbon electrocatalysts decreases the accessibility of water and destabilizes H_2O_2 molecule. In acidic electrolytes, this model implies that both 2e⁻ and 4e⁻ ORR are thermodynamically feasible, but the 2e⁻ pathway is kinetically favored; whereas in alkaline electrolyte, the 4e⁻ ORR pathway is both thermodynamically and kinetically favored. This model can be generalized to understand the pH-dependent selectivity of N-doped graphitized carbon materials.

Given that the adsorption barrier of oxygen molecules is high on the surfaces of carbon materials, alternative mechanisms that consider the interaction between O_2 molecules and hydrogen (H) site on carbon materials have been developed [60]. Different from metal-catalyzed ORR where H_2O_2 is formed by O_2 adsorption and subsequent reduction (ad-O_2 mechanism), on carbon materials, the O_2 molecule could abstract a catalyst H site to form OOH radical (or OOH^-) and undergo reduction reaction by decoupled proton-electron transfer process (Fig. 2d). The OOH^- ion mechanism is probably dominant in acidic media, as it is thermodynamically more favorable than OOH radical mechanism and kinetically more favorable than ad-O_2 mechanism by around 0.3 eV [60]. The maximum limiting potential of OOH^- ion mechanism under standard condition (0.36 V) agrees well with experimental values (0.40 V) of metal-free carbons in acidic media [60]. For non-standard conditions, the limiting potential is estimated to be 0.44 V and can be altered by the ratio between sp^2 and sp^3 hybridization. However, hydrogenation to O_2 by the surface H sites is less preferred with the increase in pH, and the ad-O_2 mechanism that promotes H_2O production dominates in alkaline media. On the other hand, the interaction between *OOH and hydrogen (proton) in the electrolyte was also proposed to rationalize the pH dependence of ORR selectivity on metal-free carbons [61]. Carbon catalysts prefer proton adsorption to the latter O atom in *OOH, resulting in immediate stabilization of OH^- and the breaking of O–OH bond. The energy barrier of O–OH bond breaking is lowered by 0.14 eV in the presence of protons (acidic condition) compared with systems without proton (neutral or alkaline condition), thus explaining the low H_2O_2 selectivity of carbon materials in acidic condition. In short, the diverse conclusions drawn from pH-effect models imply that more factors need to be considered for a thorough understanding of ORR mechanism on carbon materials in different electrolytes.

In summary, the pH effects for noble metal materials, transition metal SACs and carbon-based materials are different. Briefly, noble metals are the most active ORR catalysts and tend to be more selective for 2e⁻ pathway in acidic media than in alkaline media. The pH effect for SACs is complex, which depends on the metal center, coordination structure and chemical states of substrate. Carbon-based materials can exhibit similarly high H_2O_2 selectivity in both acidic and alkaline electrolytes, but are limited by poor activity in acids and thus suitable to produce H_2O_2 in alkaline media. The different pH-related behaviors among catalysts are explained by their difference in ORR mechanisms. Metal catalysts typically perform ORR through two PCET steps with *OOH intermediate [24], whereas alternative mechanisms, such as OOH^- ion mechanism [60], have been proposed for carbon materials. However, as there are several exceptions to the above-mentioned pH

effects, the relationship between electrolyte pH and catalytic performance still needs further development.

3. Electrocatalysts for acidic H_2O_2 production from ORR

Electrochemical H_2O_2 production from $2e^-$ ORR requires catalysts that meet several criteria, including high ORR activity, high H_2O_2 selectivity, high electrical conductivity, long-term durability, fast mass transport and low cost. Early studies of $2e^-$ ORR catalysts were mainly performed in alkaline media; however, the base-catalyzed H_2O_2 decomposition largely hinders its practical application. As such, searching for suitable $2e^-$ ORR catalysts in acidic media has attracted much attention recently. The most studied heterogeneous electrocatalysts toward acidic H_2O_2 production can be categorized as noble-metal based catalysts, non-noble-metal SACs, non-noble-metal compounds and metal-free carbon materials. This section provides a comprehensive overview of electrocatalysts that have achieved decent catalytic performance in acidic media, and some of the most representative findings are highlighted in Fig. 3 as a timeline.

3.1. Noble-metal based catalysts

Noble-metal materials are the state-of-the-art catalysts for electrochemical H_2O_2 production in acidic media in terms of their small ORR overpotentials, high H_2O_2 selectivity and good stability under operating conditions [17]. Strategies to regulate the geometric structure in aspects of active site isolation, particle size, mass loading and inter-particle distance prove effective to tune the selectivity of pure metals [62–64]. Moreover, as monometallic nanoparticles are often inefficient in H_2O_2 electrocatalysis, electronic structure modulation by alloying with a secondary metal is effective to tune the binding energy of *OOH and prevent O–O bond dissociation for desired $2e^-$ selectivity [35].

3.1.1. Noble-metal based nanoparticles

Regulating the geometric structure. Pure noble-metal nanoparticles of Au, Pt and Pd have been widely investigated for $2e^-$ and $4e^-$ oxygen reduction. Among them, Au is most suitable for H_2O_2 formation since it resides the right leg of the volcano-type activity plot and binds *OOH weakly [35]. Au-based catalysts such as Au/Vulcan XC-72R [65] and $Au_{25}(SC_{12}H_{25})_{18}$ nanoclusters [66] have been found to catalyze $2e^-$ ORR experimentally. However, the weak binding of *OOH on Au means low ORR activity and large overpotential. For pure Pt and Pd nanoparticles with strong binding of *OOH and high activity, their selectivity toward $2e^-$ ORR can be improved by regulating the surface geometry and accessibility of active sites. It is shown that by controlled carbon coating on Pt surface, the surface Pt sites are partially blocked and ORR selectivity is changed to $2e^-$ pathway (Fig. 4a) [62]. Due to steric hindrance effect, carbon coating decreases the availability of adjacent Pt sites and suppresses side-on adsorption mode of O_2. Instead, the thermodynamically unfavored end-on O_2 adsorption is forced on isolated sites, which facilitates selective H_2O_2 formation. Owing to the isolated sites, the carbon-coated Pt exhibited an onset potential of ~0.7 V vs RHE and enhanced $2e^-$ selectivity of 41% [62].

The size of nanoparticle is another critical parameter in electrocatalytic $2e^-$ ORR. Smaller nanoparticles have larger surface to volume ratio and more exposure of active sites, which would entail better electrocatalytic activity. For example, electrodeposited sub-5 nm amorphous Pd nanoparticles have shown > 95% H_2O_2 selectivity across 0–0.6 V vs RHE with high partial kinetic current densities [63]. The lack of crystalline order also plays an important role in accelerating H_2O_2 synthesis. This versatile *in situ* synthesis can be used to derive ultra-small Pt particles with high tunability toward $2e^-$ ORR [63]. Besides, the mass loading of nanoparticles and inter-particle distance have great influence on the accessibility of active sites and thus H_2O_2 performance. It is discovered that ORR selectivity shifts from $2e^-$ to $4e^-$ pathway with the increase in Pd nanoparticles loading and decrease in inter-particle distance [64]. The degree of particle dispersion clearly impacts product selectivity with more H_2O_2 formed on highly isolated sites, owing to the favored end-on adsorption configuration and enhanced release of H_2O_2 product [62].

Optimizing the electronic structure. The interaction between O_2 molecule and mono-metal surfaces is not ideal. This has stimulated interest in alloying a host noble-metal with a secondary metal to

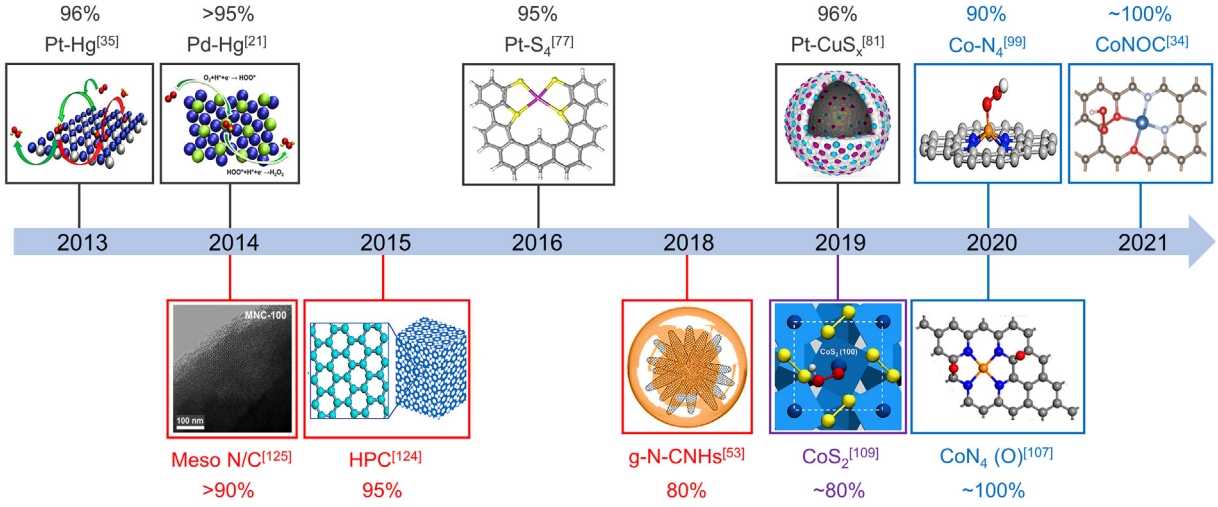

Fig. 3. Timeline of some significant findings of $2e^-$ ORR electrocatalysts in acidic media. The corresponding values of the highest H_2O_2 selectivity are provided for each catalyst. Grey: noble-metal based catalysts. Reprinted from Ref. [35] with permission from Springer Nature; Reprinted from Ref. [21] with permission from the American Chemical Society. Reprinted from Ref. [77] with permission from Springer Nature. Reprinted from Ref. [81] with permission from Elsevier. Blue: non-noble-metal SACs. Reprinted from Ref. [99] with permission from Elsevier. Reprinted from Ref. [107] with permission from Springer Nature. Reprinted from Ref. [34] with permission from the American Chemical Society. Purple: non-noble-metal compounds. Reprinted from Ref. [109] with permission from the American Chemical Society. Red: metal-free carbon-based catalysts. Reprinted from Ref. [125] with permission from the American Chemical Society. Reprinted from Ref. [124] with permission from Wiley VCH. Reprinted from Ref. [53] with permission from Elsevier.

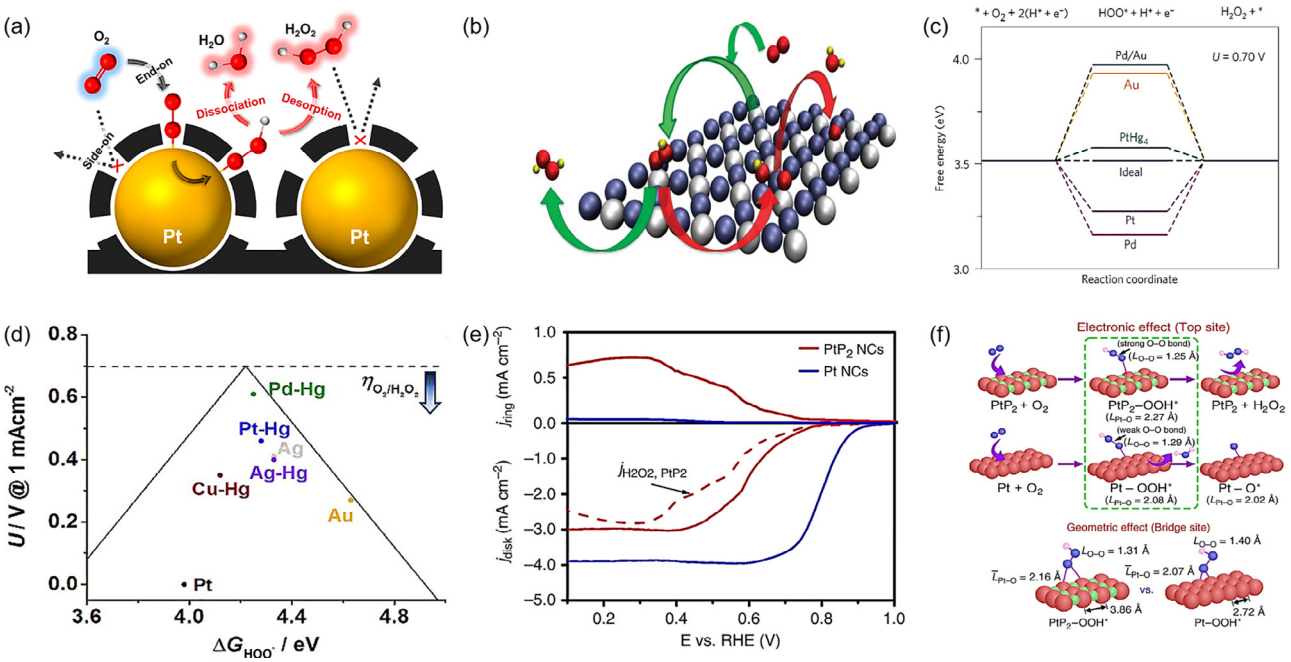

Fig. 4. Noble-metal nanoparticles for electrochemical H_2O_2 production in acidic media. (a) End-on adsorption of O_2 molecule and H_2O_2/H_2O formation on carbon-coated Pt nanoparticles. Reprinted from Ref. [62] with permission from the American Chemical Society. (b) Schematic illustration and (c) free energy diagram of $PtHg_4$ (110) surface for selective oxygen reduction to H_2O_2. Reprinted from Ref. [35] with permission from Springer Nature. (d) Pd-Hg alloy for electrocatalytic H_2O_2 production. Reprinted from Ref. [21] with permission from the American Chemical Society. (e) Polarization curves of PtP_2 nanocrystals in O_2-saturated 0.1 M $HClO_4$ at 1600 rpm. (f) Enhanced 2e⁻ ORR selectivity on PtP_2 nanocrystals by geometric and electronic effects. (e and f) are reprinted from Ref. [72] with permission from Springer Nature.

induce electronic effects and tune the binding energy of ORR intermediates toward optimal level [35]. According to Sabatier's principle, this level corresponds to the peak of 2e⁻ ORR volcano plot where the binding of *OOH (or *OH) is neither too strong nor too weak, such that O_2 can be actively and selectively reduced to H_2O_2. As Pt and Pd bind *OOH too strongly, alloying with a catalytically inactive weak-binding metal is a possible way to improve their H_2O_2 selectivity. In 2013, Siahrostami et al. identified that $PtHg_4$ is a promising candidate for H_2O_2 electrosynthesis by DFT calculations with a thermodynamic overpotential lower than 0.1 V (Fig. 4b and 4c) [35]. Electrochemical measurements confirmed that in 0.1 M $HClO_4$, Pt-Hg alloy shows a H_2O_2 selectivity of up to 96% and a mass activity of 26 ± 4 A $g^{-1}_{noble\ metal}$ at an overpotential of 50 mV. Following this, the same group also screened other metals with Hg-modified surface and discovered that Pd-Hg and Ag-Hg outperform Pt-Hg for H_2O_2 production [21]. Notably, Pd-Hg is situated closer to the peak of the volcano plot than previously reported Pt-Hg with five times higher activity per mass of precious metal, making it the state-of-the-art noble-metal catalyst for H_2O_2 production in acidic media (Fig. 4d). Due to the toxicity of Hg, this alloying approach has also been extended to other Hg-free systems, including Au-Pd nanoparticles [67,68], PdAu nanoframes [69], and atomically dispersed Pt@AuCu [70]. Because Au binds *OOH relatively weakly, alloying Au with the strong-binding Pd is promising to achieve better electrocatalytic performance. For example, PdAu nanoframes prepared by controlled solution growth and etching exhibited much enhanced onset potential (~0.56 V vs RHE) and H_2O_2 selectivity (> 90%) in acid superior to pure Au and other Au alloys [69]. The introduction of dilute Pd atoms to PdAu nanoframes could stabilize the adsorption of *OOH through direct Pd–O bonding, which was identified as the origin of enhanced 2e⁻ ORR performance.

Furthermore, the interplay between electronic effect and geometric site isolation effect is more advantageous to boost H_2O_2 activity and selectivity. For example, the partially oxidized Pd clusters with an average size of 0.61 nm loaded on oxidized carbon nanotube ($Pd^{\delta+}$-OCNT) were reported to manifest 95–98% selectivity for H_2O_2 production and unprecedented mass activity of 1.946 A mg^{-1} in acidic media [71]. It has been revealed that the exceptional 2e⁻ ORR performance originates from the interaction between small Pd clusters (Pd_3 and Pd_4) and epoxy functional groups of carbon, which moves the catalyst toward the apex of thermodynamic volcano plot. In another work, platinum diphosphide (PtP_2) nanocrystals synthesized by hot-injection method displayed 98.5% H_2O_2 selectivity at 0.27 V vs RHE with negligible overpotential (Fig. 4e) [72]. DFT calculations implied that P is responsible for lowering the end-on adsorption energy of O_2 molecule and weakening the binding strength of Pt–OOH*, rendering PtP_2 highly selective for 2e⁻ ORR (Fig. 4f). Very recently, it has been reported that alloying Pd with semi-metal Se could derive Pd_4Se nanoparticles for pH-universal H_2O_2 electrosynthesis [73]. $PdSe_4$ outcompeted commercial Pd/C and Pd-based nanoparticles in terms of better H_2O_2 selectivity (93.5%) in 0.1 M $HClO_4$ and durability after 5000 cycles. The incorporation of Se atoms leads to both geometric effect and electronic effect for the remarkable performance. The isolated Pd atoms by Se would favor end-on adsorption of oxygen, and the strong p-d repulsion promotes mismatch of O-2p band to stabilize *OOH, both of which are favorable factors for 2e⁻ ORR process.

3.1.2. Noble-metal single-atom catalysts

Recently, single-atom catalysts have attracted great attention for their unique structure and outstanding performance in electrocatalytic H_2O_2 production [22]. Unlike their bulk nanoparticle counterparts, SACs usually contain atomically dispersed metal atoms over metal compounds or carbon-based substrates, and the utilization efficiency of metal is thus maximized (~100%) [74]. Their well-defined active centers allow clear characterization of structure-property relationships, while the electronic structure of SACs can be modified by tuning metal atoms and their coordina-

tion environment [22,75]. More importantly, SACs are intrinsically suitable for selective 2e⁻ ORR in terms of the adsorption configuration of oxygen molecules. As discussed in Section 2, the isolated metal sites in SACs would favor end-on (Pauling-type) adsorption of O_2 instead of side-on adsorption. For end-on adsorption, the axis of O–O bond is vertical to the material surface, which lowers the possibility of O–O bond dissociation and is beneficial for the desorption and release of H_2O_2.

In acidic solution, Pt is a well-known 4e⁻ ORR catalyst; however, similar to active site isolation of nanoparticles, the selectivity can be shifted to 2e⁻ pathway when Pt is dispersed on atomic scale [76–78]. For example, Choi et al. synthesized atomically dispersed Pt catalysts (5 wt%) embedded in sulfur-doped zeolite-templated carbon (ZTC) using a facile wet-impregnation method. The sample achieved selective H_2O_2 production in 0.1 M $HClO_4$ with an electron transfer number of 2.1 and H_2O_2 production rate of 97.5 μμmol h^{-1} cm^{-2} in an electrochemical H-cell reactor [77]. This performance is ascribed to the unique structure of Pt SACs compared with bulk Pt nanoparticles, as polycrystalline Pt surface would favor further reduction of H_2O_2 [79]. The substrate also plays a crucial role in affecting the ORR selectivity of Pt SACs. Pt single atoms supported on titanium carbide (Pt_1/TiC) showed higher activity, selectivity and stability for electrocatalytic H_2O_2 production than those on titanium nitride (Pt_1/TiN) (Fig. 5b) [80]. DFT analysis explained that Pt_1/TiC prevents the O–O bond from dissociation, whereas Pt_1/TiN affords strong affinity of oxygen species and poisons the catalyst surface. Therefore, it is important to carefully select the substrate when designing SACs, as it not only provides anchoring sites for metal atoms but also directly tunes the electrocatalytic ORR pathway. In addition, SACs are often plagued by limitations in metal loading and thus low activities. If the amount of isolated active sites is increased, the resulting catalysts can achieve desired selectivity without compromising their electrochemical activity. For example, Shen et al. designed a novel ion exchange method to prepare single atomic Pt supported on amorphous CuS_x with an exceptional concentration of Pt (24.8 at %) (Fig. 5c) [81]. The obtained sample achieved a high H_2O_2 selectivity of 92%–96% over a wide potential range of 0.05–0.7 V vs RHE and a great kinetic H_2O_2 generation mass activity of 35 A mg_{cat}^{-1} at 0.4 V vs RHE in 0.1 M $HClO_4$ electrolyte.

Apart from Pt, noble metals such as Au and Pd SACs also exhibit great potential toward 2e⁻ ORR pathway in acidic media. By combining DFT calculations and experiments, Sahoo et al. investigated transition metal M-SACs (M = Cu, Ag, Au, Ni, Pd or Pt) supported on TiC substrates and demonstrated that Au and Pd SACs are more promising for acidic H_2O_2 production than Pt SACs [82]. At applied potential of 0.2 V vs RHE, the H_2O_2 selectivity of Au and Pd SACs are 87% and 80%, respectively, compared to 71% of Pt SACs. The promoting effect of Pd single atoms for H_2O_2 production was also shown in a report by Jirkovský et al., where the increase of atomically dispersed Pd content to 8 wt% in Au nanoparticles results in corresponding increase in H_2O_2 selectivity (up to 95%) [83]. The selectivity improvement is attributed to the isolated surface Pd atoms present in $Au_{1-x}Pd_x$ nanoalloys that favor side-on adsorption of oxygen and thus selective 2e⁻ ORR process (Fig. 5d) [83]. Pd supported on $C@C_3N_4$ [84], Pd bound with defect graphene [85] and $PdCl_x$/C [86] are also among the Pd SACs with high H_2O_2 selectivity. In another work, Kim et al. designed a general strategy to synthesize noble metal (Os, Ru, Rh, Ir and Pt) SACs by immobilizing metal precursors in carbonaceous coating and SiO_2 layer [87]. It was discovered that the binding energy difference between *OOH and *O governs the H_2O_2 selectivity, with the Rh SACs possessing the best ORR activity and Pt SACs showing the highest selectivity. In summary, compared to noble-metal nanoparticles, noble-metal SACs with isolated active sites favor end-on O_2 adsorption and H_2O_2 formation due to the lack of neighboring sites. The selectivity toward 2e⁻ ORR can be further tailored by the type and content of metal center, coordination structure, and support matrix.

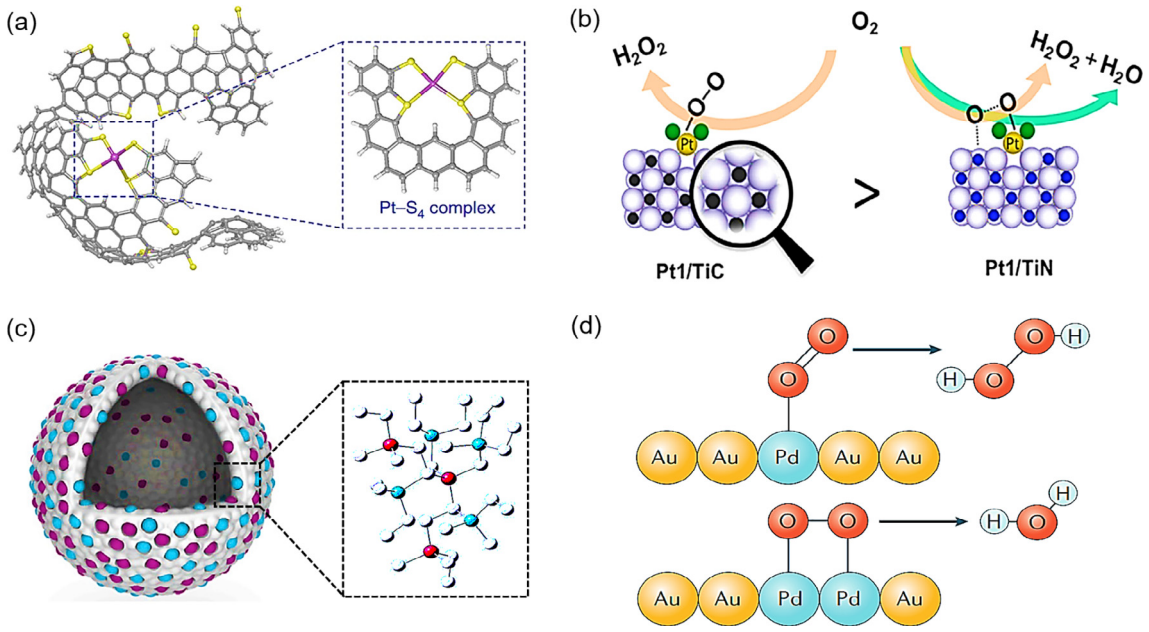

Fig. 5. Noble-metal single-atom catalysts for electrochemical H_2O_2 production in acidic media. (a) Atomically dispersed Pt catalysts in sulfur-doped zeolite-templated carbon. Reprinted from Ref. [77] with permission from Springer Nature. (b) Schematic illustration of the support effect in Pt SACs with high H_2O_2 selectivity for Pt_1/TiC. Reprinted from Ref. [80] with permission from the American Chemical Society. (c) Schematic illustration of highly concentrated Pt single atoms embedded in amorphous CuS_x support. Purple: Pt; Blue: Cu; White: S. Reprinted from Ref. [81] with permission from Elsevier. (d) Pd single atom hotspots at $Au_{1-x}Pd_x$ nanoalloys for selective H_2O_2 production. Reprinted from Ref. [5] with permission from Springer Nature.

3.2. Non-noble-metal single-atom catalysts

Non-noble-metal SACs are emerging as alternatives to replace noble-metal based catalysts in a wide range of electrocatalytic reactions [74,88–90]. In ORR, while the most explored metal-nitrogen-carbon (M-N-C) type SACs have offered excellent performance comparable to that of noble-metal based catalysts toward $4e^-$ process, fewer studies have focused on tuning the selectivity to produce H_2O_2 [91–93]. The structure-property relationship of SACs is dependent on metal centers, local coordination environments and host matrix, which makes the rational design of selective catalysts more elusive than previously thought [94]. Without a clear identification of real active sites and catalytic mechanism, the reported performances of SACs are sometimes contradictory even for the same catalyst. For example, Co-N-C SACs have been reported as promising candidates for fuel cell applications due to their outstanding $4e^-$ ORR performance [95–98], yet a few studies also show their ability to selectively catalyze $2e^-$ ORR [99,100]. For this reason, it is necessary to acquire atomic-level insights into SACs design for H_2O_2 electrocatalysis.

At the atomic level, transition-metal based SACs usually consist of atomically dispersed metal centers coordinated in a carbon-based matrix. This chemical feature combines the advantages of both homogeneous catalysts and heterogeneous catalysts, exhibiting high electrochemical activity without compromising durability. The structure of SACs has been compared with naturally occurring metalloenzyme systems, which offers unique and comprehensive understanding of active sites in electrocatalytic reactions [34,100–102]. Metalloenzymes are comprised of metal centers, the immediately surrounding organic ligands (first coordination sphere) and ligands bonding to the first coordination sphere (second coordination sphere) [103]. Analogously, the catalytic performance of SACs can be collectively influenced by metal center, atoms in the first coordination sphere and functionalization in the second coordination sphere (Fig. 6a) [34]. Thus, regulation of these components is expected to derive SACs with desired acidic ORR activity and selectivity [104,105].

3.2.1. Regulation of metal center and first coordination sphere

The ORR selectivity of SACs largely depends on the central metal atom. In most cases, metal center is the active site that does the catalysis, and its careful selection is able to achieve appropriate binding of ORR intermediates for desired $2e^-$ selectivity. Sun et al. investigated the effect of 3d metal on the $2e^-$ ORR activity and selectivity of M-N-C (M = Mn, Fe, Co, Ni, Cu) SACs [47]. Co-N-C was found to be the optimal catalyst due to its highest ring current for ORR (0.18 mA at 0.1 V vs RHE), highest selectivity for acidic H_2O_2 production (80% at 0.1 V vs RHE) and lowest activity for H_2O_2 reduction (Fig. 6b). In another study, the Co-N-C anchored in N-doped graphene was also identified as ideal $2e^-$ ORR catalyst exceeding the performance of state-of-the-art noble-metal based catalysts [99]. In 0.1 M $HClO_4$, the kinetic current of Co SACs reached 1 mA cm^{-2} at 0.6 V vs RHE with H_2O_2 Faradaic efficiency > 90%, as well as stability for a period of 10 h. DFT calculations revealed that the binding energies of ORR intermediates over transition metals increase with the number of valence electron, and Co SACs has the optimized binding energy of *OOH, rendering Co–N_4 motif the active site for H_2O_2 production (Fig. 6c) [99]. To confirm the crucial role of metal centers, Liu et al. adjusted the metal centers in SACs while controlled the coordination environment by the same porphyrin moieties using well-defined covalent organic framework models [106]. They drew similar conclusion that Co is the most intrinsically active, and showed that difference in binding energy of $*O_2$ and *HOOH could serve as a new descriptor to evaluate the activity of SACs.

Introducing metals into carbon skeleton inevitably induces changes in the electronic structure of neighboring atoms. Therefore, beyond controlling metal centers, regulating first coordina-

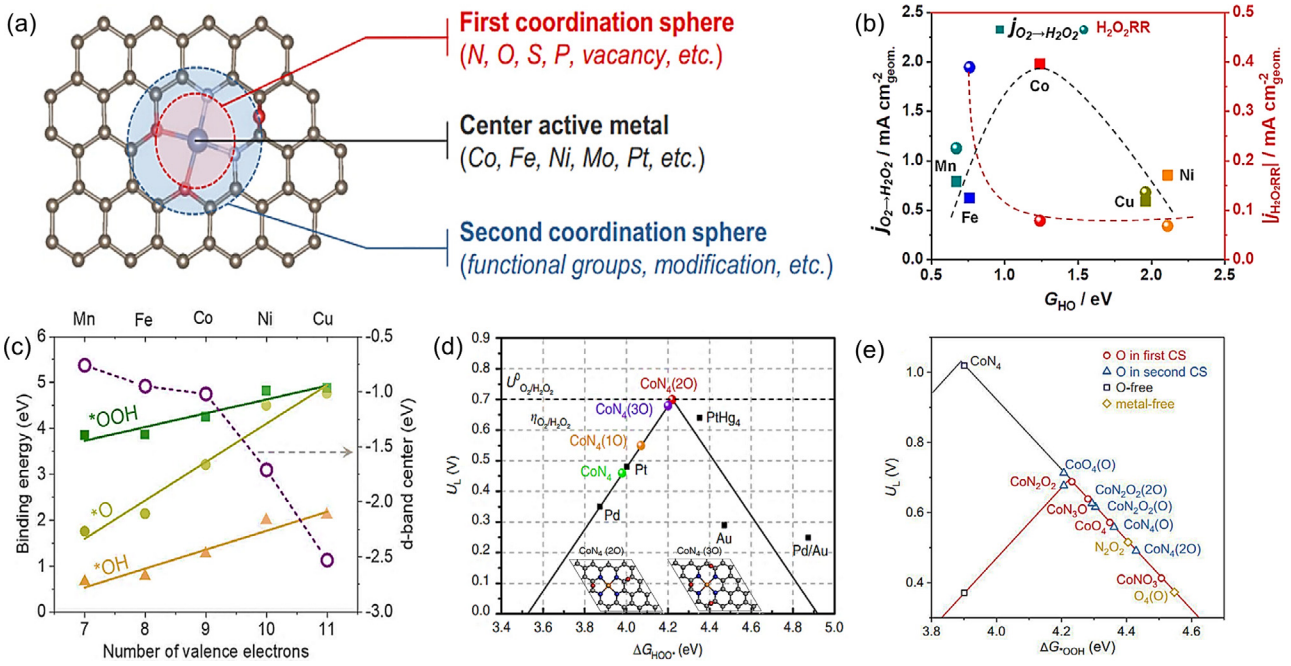

Fig. 6. Non-noble-metal single-atom catalysts for acidic H_2O_2 production. (a) Schematic illustration of SACs. Reprinted from Ref. [34] with permission from the American Chemical Society. (b) Thermodynamic activity and selectivity trends of ORR as a function of *OH binding energy on M-N-C catalysts. Reprinted from Ref. [47] with permission from the American Chemical Society. (c) Binding energies of *OOH, *O and *OH and d-band center of metal atom in M-N-C SACs (M = Mn, Fe, Co, Ni, Cu). Reprinted from Ref. [99] with permission from Elsevier. (d) Schematic illustration of geometric structures and activity volcano plot of CoN_4 with different epoxy group coverage. Reprinted from Ref. [107] with permission from Springer Nature. (e) ORR activity volcano plot for Co SACs with various configurations in the first and second coordination spheres. Reprinted from Ref. [34] with permission from the American Chemical Society.

tion sphere is deemed important for H_2O_2 production as well. By varying center atoms (Fe, Pd, Co, Mn) and adjacent coordination atoms (N, O, C), researchers established a trend in ORR pathway and elucidated the effect of metal centers and first coordination sphere in alkaline media [30]. Fe-C-O motif displays the best performance for H_2O_2 generation with the highest H_2O_2 selectivity > 95%; in contrast, when the coordinating atom is changed to N, Fe-C-N motif becomes selective for $4e^-$ ORR. Similarly, Mo SACs with sulfur and oxygen dual-coordination could tune the adsorption behavior toward $2e^-$ ORR in alkaline electrolytes [75]. Single-atom Mo complex is the active origin of $2e^-$ ORR, whereas atoms in the first coordination sphere (Mo–S_4–C and Mo–O_3S–C) greatly affect the reaction pathway. It is noticeable that the resultant Mo SACs have a high metal loading of > 10 wt% without agglomeration, which represents a promising strategy for large-scale synthesis of high-loading SACs toward high activity and selectivity. The above studies were mainly conducted in alkaline media, but it is expected that strategies to engineer first coordination sphere are also applicable for acidic H_2O_2 production.

3.2.2. Regulation of second coordination sphere

Although second coordination sphere does not directly interact with metal center, recent studies have shown its importance in fine-tuning the adsorption configurations and affecting catalytic behaviors. Jung et al. found that the *OOH binding on Co-N-C SACs could be tuned by the surrounding atomic configuration of Co [100]. Specifically, introducing electron-deficient *H or electron-rich *O has different effects on the charge state and ORR intermediate binding energy of Co-N_4/graphene moieties. When oxygen groups are attached near Co–N_4 to form Co–N_4(O), ΔG_{*OOH} increases from 3.9 eV to 4.1 eV, becoming closer to the peak of volcano where ΔG_{*OOH} = 4.2 eV. When the electron-poor hydrogen groups are adsorbed, ΔG_{*OOH} decreases from 3.9 eV to 3.8 eV. As such, it is possible to fine-tune the electronic structure of Co–N_4 in the second coordination sphere. Guided by insights from theoretical prediction, the researchers synthesized Co_1–NG(O) with electron-rich oxygen species (such as C–O–C) surrounding Co centers, resulting in selective H_2O_2 production in 0.1 M $HClO_4$. Furthermore, the role of surface epoxy groups in the second coordination sphere was also confirmed by another research group (Fig. 6d) [107]. In acidic electrolytes, Co SACs on N-doped carbon nanotubes showed previously unachieved near-zero overpotential and ~ 100% selectivity for $2e^-$ ORR. To rationalize this exceptional performance, spectroscopic analyses proved that the presence of epoxy groups near Co–N_4 centers significantly modifies the electronic structure of Co atoms, uncovering the synergy between Co–N_4 and second coordination sphere (epoxy O).

Very recently, the synergetic modification of first coordination sphere and second coordination sphere has been reported to optimize electrocatalytic $2e^-$ ORR of SACs in acidic media (Fig. 6e) [34]. Theoretically, similar to metalloenzymes, changes in the first and second coordination spheres of SACs affect the electronic structures and intermediate adsorption behavior. In Co SACs, Co atoms coordinated with N and O (CoNOC) exhibited H_2O_2 selectivity of > 95%, in sharp contrast to the low selectivity < 30% over pure N-coordinated catalyst (CoNC) [34]. The combined calculations and *in situ* infrared absorption spectroscopy confirmed that both first and second coordination spheres are critical to the performance of SACs. In the first coordination sphere, different coordinating atoms (N, O, etc.) could modulate the binding energy of *OOH on Co centers, as witnessed by the selectivity difference of CoNC and CoNOC. Introducing O atom into first coordination sphere (Co–N_x) weakens the adsorption of *OOH, and shifts the active sites from Co center to the nearby O-adjacent carbon. In the second coordination sphere, Bader charge analysis revealed a negative relationship between ΔG_{*OOH} and charge state of catalytic active carbon atoms. The CoO_4(O) is an exception, where the out-of-plane epoxy group exerts steric hindrance to stabilize *OOH binding as confirmed by charge difference analysis. This work highlights the molecular-level design principles of SACs for efficient electrocatalysis.

3.3. Non-noble-metal compounds

Apart from non-noble-metal SACs, a number of non-noble-metal compounds have also been investigated for acidic $2e^-$ ORR process, such as metal chalcogenides [108–113], metal oxides [114–116], metal-organic framework [117], and hybrids [118]. The activity, selectivity and stability toward H_2O_2 production are highly dependent on their nanostructure, morphology, composition and exposed facets. Furthermore, these compounds are often supported on carbon materials to enhance conductivity and better isolate active sites, which can optimize adsorbate binding and thus improve their catalytic performance. For example, Sheng et al. reported a combined experimental and computational study to demonstrate that cobalt pyrite (CoS_2) is an active and selective $2e^-$ ORR electrocatalyst in acidic and neutral solutions [109]. In 0.05 M H_2SO_4, CoS_2 drop-casted on RRDE showed its intrinsic H_2O_2 selectivity peaking at 70%–80%, while CoS_2 nanowires supported on carbon fibers paper showed a selectivity of ~70% at 0.5 V vs RHE in bulk ORR electrolysis. Computation modelling revealed that this performance is attributed to the modest binding of *OOH on the isolated Co site of CoS_2 (100) facet and the suppressed O–O bond cleavage in kinetics. In a more recent work, the same group discovered that two structural polymorphs of cobalt diselenide ($CoSe_2$), i.e. the cubic pyrite-type (*c*-$CoSe_2$) and the orthorhombic marcasite-type (*o*-$CoSe_2$), are selective for H_2O_2 electrosynthesis and stable against catalyst leaching [110]. Surface Pourbaix diagrams confirmed the weak binding of *O to Se sites and better stability of Co atoms than those in CoS_2. In electrochemical H-cell setup, *o*-$CoSe_2$ nanowires grown on carbon paper electrodes achieved an accumulated H_2O_2 concentration of 547 ppm in 0.05 M H_2SO_4 and enabled electro-Fenton process for rhodamine B degradation. Besides metal chalcogenides, other metal compounds can also be endowed with high activity and selectivity toward acidic H_2O_2 production. For example, Gao et al. engineered the crystal facets and oxygen vacancies to activate the inert hematite (α-Fe_2O_3) for selective H_2O_2 production [115]. DFT calculations found that the oxygen-defective (001) facet of α-Fe_2O_3 is promising for H_2O_2 production by preventing O–O bond cracking. The rich oxygen vacancies favor end-on adsorption of oxygen and subsequent protonation to produce H_2O_2. Electrochemical experiments verified that single-crystal with exposed (001) facets exhibited > 90% selectivity in weakly acidic solution (5 mM H_2SO_4), providing a feasible catalyst with earth-abundant elements in electrosynthesis.

Remarkably, Co-based nanomaterials are a class of unique candidates for acidic H_2O_2 production. Co nanoparticles encapsulated within N-doped graphitic carbon were reported to trigger H_2O_2 synthesis in acidic media with almost 100% Faradaic efficiency and production rate of 49 mmol g^{-1} h^{-1} [119]. The ability to synthesis H_2O_2 in acidic media is related to a combination of factors, including pH values, applied potential, porosity and distribution of N moieties. In another study, it was found that cobalt-triethylenetetraamine complex pyrolyzed at different temperatures (Co/TETA/C) exhibits a rise in H_2O_2 yield from 60% to nearly 100% in 0.1 M $HClO_4$ when the pyrolysis temperature is below 500 °C [120]. Temperature exceeding 500 °C is detrimental to H_2O_2 yield because of the formation of metallic cobalt particles. A detailed kinetic analysis confirmed that the reaction mechanism of obtained cobalt-containing catalysts is unchanged whether Co is in metallic or Co(II)-like form after heat treatment. Cobalt phthalocyanine (CoPc) compounds can also act as modifier of carbon mate-

rials for enhanced H_2O_2 production in acidic media, leading to a maximum H_2O_2 Faradaic efficiency of 92.3% with 1 wt% CoPc modification and a positive overpotential shift of 340 mV with 10 wt% CoPc modification [121]. Despite these advances in non-noble-metal compounds for acidic H_2O_2 electrosynthesis, further efforts to regulate their active centers, refine the mechanism understanding, and improve long-term stability are urgently needed.

3.4. Metal-free carbon-based catalysts

In contrast to metal-based catalysts, metal-free carbon-based materials are regarded as highly promising electrocatalysts due to their earth abundance, low cost, high surface area, good electrochemical stability and electrical conductivity [122,123]. In acids, the ORR activity of pristine carbon materials is low because of the intrinsically weak adsorption of *OOH intermediate. Therefore, it is imperative to create active sites in carbon frameworks by means of morphology control and heteroatom functionalization.

3.4.1. Morphology control

Morphology control strategies by defect and pore engineering have been reported to boost electrochemical acidic H_2O_2 production of carbon catalysts [124,125]. Topological defective sites naturally exist and can be facilely introduced to sp^2 carbon planes during physical and chemical synthesis [126]. These defects, including disorders, in-plane vacancies and edge sites, can effectively alter the electronic structure of carbons [127]. For example, Liu et al. performed carbonization of MOF-5 precursor under H_2 atmosphere to introduce sp^3 type defects into hierarchically porous carbon (HPC) [124]. The rich sp^3-C bonds and defects can serve as active sites for adsorption and reaction of oxygen. More importantly, the H_2O_2 production rates were found to increase with the intensity ratio of D and G bands in Raman spectra (I_D/I_G), indicating that defect may facilitate H_2O_2 production (Fig. 7a). For the optimized HPC-H24 catalyst (hydrothermal treatment for 24 h and pyrolysis under H_2 atmosphere), the H_2O_2 selectivity is 80.9%–95.0% in acidic media at potential range of –0.1 V to –0.5 V vs saturated calomel electrode (SCE) (Fig. 7b), and the current efficiencies for H_2O_2 production are 85.2%–91.2%

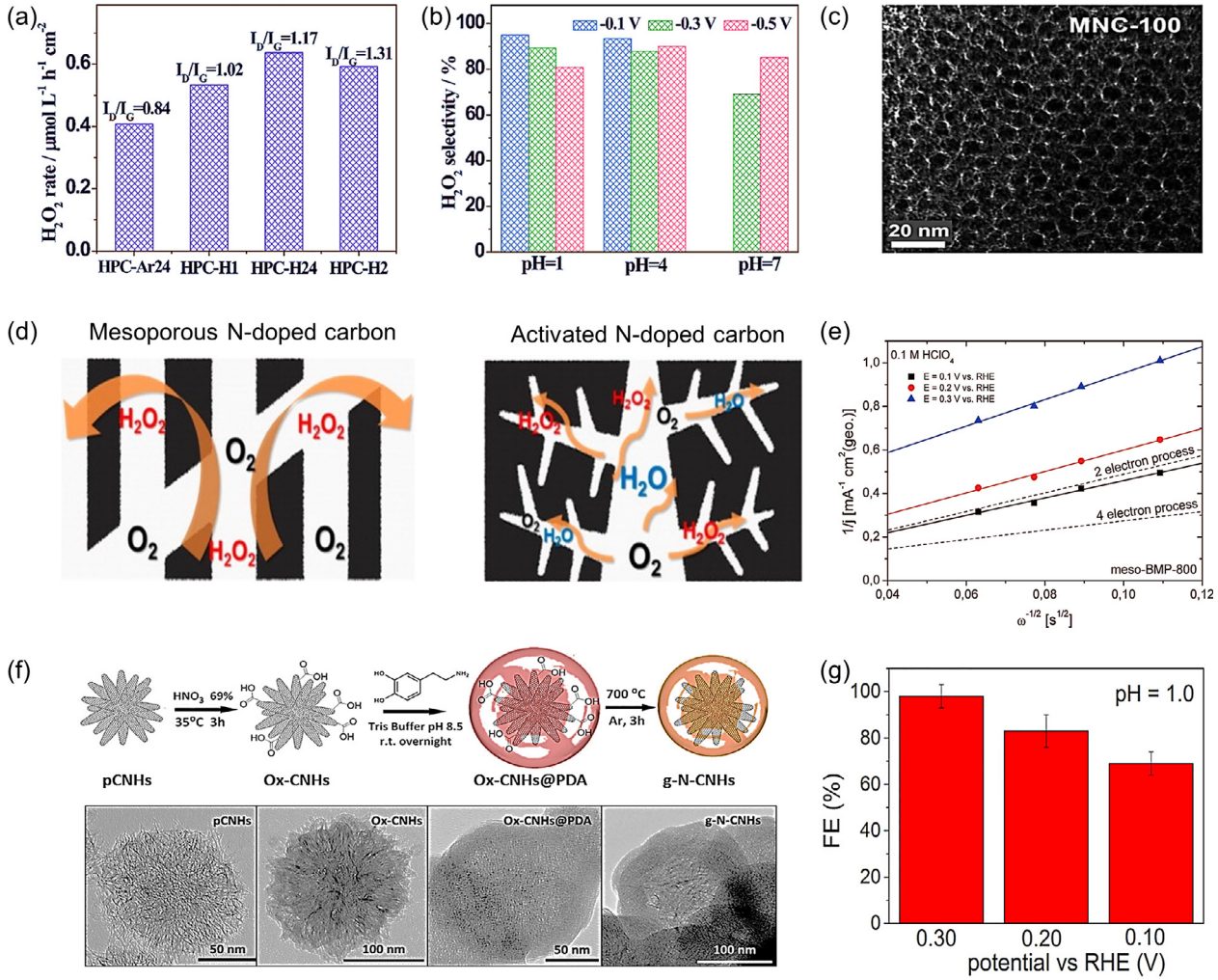

Fig. 7. Metal-free carbon-based materials for electrochemical H_2O_2 production in acidic media. (a) H_2O_2 production rates and I_D/I_G ratio of hierarchically porous carbon. (b) H_2O_2 selectivity of HPC-24 at pH value of 1, 4 and 7 and applied potential of –0.1 V, –0.3 V and –0.5 V vs SCE. (a and b) are reprinted from Ref. [124] with permission from Wiley VCH. (c) Transmission electron microscopy (TEM) image of mesoporous nitrogen-doped carbon synthesized from 100% (1-methyl-1H-pyrrole-2-yl)methanol precursor. (d) Schematic illustration of ORR pathways on mesoporous nitrogen-doped carbon and micropore-dominant activated nitrogen-doped carbon. (c and d) are reprinted from Ref. [125] with permission from the American Chemical Society. (e) Koutecky-Levich plot of meso-BMP-800 in 0.1 M $HClO_4$. Reprinted from Ref. [132] with permission from the American Chemical Society. (f) Synthetic diagram of g-N-CNHs and related TEM images at intermediate stages during synthesis. (g) H_2O_2 Faradaic efficiency of g-N-CNHs electrode at pH of 1 and different potentials. (f and g) are reprinted from Ref. [53] with permission from Elsevier.

at pH of 1 and 73.0%–82.4% at pH of 4, respectively. Similar relation between defects (represented by I_D/I_G ratio) and H_2O_2 selectivity was also unveiled for nitrogen-doped mesoporous carbon to prove that defect sites are favorable for H_2O_2 production [128]. The aliphatic-like defect sites on several commercially available carbons were revealed to increase surface hydrogen content, contributing to better 2e⁻ selectivity and Faradaic efficiency in 0.1 M $HClO_4$ [129].

Additionally, the pore structures of carbon materials greatly influence electrocatalytic selectivity by regulating active site exposure and mass transport of reactants and products. Micropores with a diameter less than 2 nm provide large surface area but are limited by low accessibility of active sites, whereas macropores (> 50 nm) display the opposite trend. Mesopores (2–50 nm) with decent surface area and mass transfer properties are most beneficial. For example, mesoporous nitrogen-doped carbon prepared by SiO_2-templated carbonization of (1-methyl-1H-pyrrole-2-yl) methanol was found to deliver H_2O_2 selectivity of over 90% in 0.5 M H_2SO_4 (Fig. 7c) [125]. By contrast, an activated nitrogen-doped carbon with microporous structure exhibited significantly lower H_2O_2 selectivity of 56–70%. The enhanced selectivity of mesoporous carbons was attributed to the ease of mass transport in the catalyst layer and reduced residence time of H_2O_2 to prevent its further reduction (Fig. 7d). A comparison between microporous and mesoporous carbons with similar physical and chemical properties except the difference in pore size, albeit in alkaline conditions, showed that mesoporous carbon demonstrated better electrochemical accessibility, activity, selectivity and stability toward H_2O_2 production [50]. It is notable that they investigated the role of carbon defects by spectroscopic characterizations and DFT calculations and revealed that most sp^2-type defect configurations are inherently selective for 2e⁻ ORR, highlighting the interplay between pore size and defect in affecting electrochemical ORR performance of carbon materials. To gain a better understanding of the structure-performance relation and guide further optimization, well-defined mesoporous carbon-based model materials and advanced simulation by finite-element method is highly anticipated [130].

3.4.2. Heteroatom functionalization

Functionalization of carbon materials with heteroatoms has become a simple yet powerful approach to tune the electronic structure of carbon for ORR application. The difference in electronegativity, atom size and chemical states of non-metal heteroatoms could induce spin and charge redistribution within sp^2 carbon and modulate the binding energies of ORR intermediates [127]. Also, the heteroatom-induced defective structure in carbon materials and the increase in surface area may contribute to enhanced 2e⁻ ORR activity and selectivity.

Nitrogen doping is the most widely reported strategy to optimize the binding strength of *OOH. From the kinetic perspective, nitrogen-doped carbon catalysts have higher kinetic rate constant of 2e⁻ ORR than 4e⁻ ORR and H_2O_2 reduction processes, indicating their high selectivity toward 2e⁻ pathway [131]. In 2012, Fellinger et al. synthesized mesoporous nitrogen-doped carbon from ionic liquid N-butyl-3-methylpyridinium dicyanamide as a highly efficient and selective catalyst for electrochemical H_2O_2 synthesis [132]. In 0.1 M $HClO_4$, meso-BMP-800 (mesoporous N-doped carbon heat-treated at 800 °C) showed an approximate 2e⁻ process by Koutecky-Levich analysis (Fig. 7e). The researchers discovered that the reactivity toward H_2O_2 depends on the nitrogen content and configuration of N-doped carbon. An increased amount of nitrogen and the "radical" character of nitrogen-bound carbon were believed to favor 2e⁻ ORR process. They found that pyrrolic nitrogen sites were responsible for 2e⁻ ORR, but higher synthesis temperature would decrease the amount of pyrrolic nitrogen and is therefore detrimental to H_2O_2 production. Iglesias et al. prepared N-doped graphitized carbon nanohorns (g-N-CNHs) through facile coating and controlled annealing of polydopamine (Fig. 7f) [53]. The catalyst could work under pH of 1.0 with a H_2O_2 Faradaic efficiency as high as 98% at 0.30 V vs RHE (Fig. 7g) and very positive onset potential of 0.40 V vs RHE. The long-term durability was confirmed by the stable H_2O_2 production rate of 33 mmol g^{-1} h^{-1} cm^{-2} over 24 h. The researchers correlated the high selectivity under acidic conditions to the microporosity for decreased residence time of H_2O_2 and the protonated pyridinic N atoms for preferentially maintained O–O bond.

The electrocatalytic performance of N-doped carbon materials can be further tuned by the nitrogen content and configurations. For example, Sun et al. unveiled a volcano-type relationship between H_2O_2 selectivity and the amount of N functionalities, suggesting that there is an optimal level of nitrogen dopant density for maximized H_2O_2 production [128]. A balanced distance of individual N dopant from each other is beneficial for 2e⁻ ORR pathway, as the excessive doping may facilitate O–O bond cleavage and H_2O_2 decomposition. Furthermore, the same research group investigated the structure-activity relationship and individual role of chemically distinct N functionalities in different electrolytes by XPS [133]. They prepared nitrogen-doped porous carbons by direct pyrolysis of ordered mesoporous carbon CMK-3 and polyethylenimine mixture, achieving a high H_2O_2 selectivity of 95.3% in acidic electrolyte. However, the H_2O_2 production rate by bulk electrolysis in acid (34.1 mmol g^{-1} h^{-1}) is lower than that in neutral electrolyte (570.1 mmol g^{-1} h^{-1}), which may be ascribed to the gradual chemical disproportionation and further electrochemical reduction. In acidic solution, the amount of pyridinic N decreased and the amount of graphitic N increased after electrocatalysis, whereas the opposite trend was observed in neutral and alkaline solutions; meanwhile, the pyrrolic N content increased irrespective of the pH values of electrolyte. Such dynamic changes in specific type of N functionality during catalysis were ascribed to the adsorbed oxygenated groups (*O and *OH). Specifically, a covalently attached OH group to a carbon atom can transform the adjacent pyridinic N into pyridonic N, while a similar OH attachment to an adjacent carbon atom of graphitic N can downshift its binding energy to that of pyrrolic N. These phenomena suggested that pyridinic N has a deterministic role in controlling acidic H_2O_2 production, while graphitic N is the catalytic active site in neutral and alkaline solutions. It should be noted that the real active sites and reaction mechanism of N-doped carbons in 2e⁻ ORR are still under debate. Despite the above evidence of pyridinic N sites for selective 2e⁻ ORR, they have also been reported to actively catalyze 4e⁻ ORR in 0.1 M H_2SO_4 [134]. Thus, determining the individual role of N configuration in acidic H_2O_2 production is an ongoing challenge. The ORR selectivity debate of N-doped carbons largely originates from the uncontrolled synthesis methods and lack of direct evidence of active sites. Existing synthesis methods typically generate multiple N configurations in one catalyst and cannot precisely control other factors that affect ORR selectivity, such as defects and porosity. In order to identify the active site and construct structure-property relationship, further work is needed to prepare well-defined platforms of N-doped carbon with single N configuration, and develop advanced *in situ* characterization techniques to probe the chemical states of N-doped carbons under operating conditions.

In addition to nitrogen dopants, doping with other heteroatoms (O, S, F, etc.) and dual-doping can also tailor the electronic structure of carbon catalysts toward acidic H_2O_2 production [51,135–140]. For example, oxidized carbon materials can incorporate various active and selective oxygen-containing functional groups to achieve outstanding 2e⁻ ORR performance. Lu et al. demonstrated that surface oxidation of carbon nanotubes by nitric acid can significantly boost their performance for electrochemical H_2O_2 pro-

duction [51]. The activity and selectivity of 2e⁻ ORR are positively correlated with oxygen content. Through DFT calculation and a series of control experiments, the researchers found that oxygen species modulate adjacent carbon atoms for optimized adsorption of *OOH, and the active sites for 2e⁻ ORR are the carbon atoms adjacent to –COOH and –C–O–C groups. To directly identify the real active sites, Han et al. studied a series of activated carbon materials with dangling edge sites and decorated with targeted functional groups, including quinone, carbonyl and etheric ring [136]. In acidic media, the quinone-enriched carbon exhibited higher selectivity (up to 97.8 % at 0.75 V vs RHE) and activity than other two counterparts, and the most active motif was determined to be the quinone functional group in the edge and basal plane of carbon. However, it is noticeable that while the oxidation of carbon materials enhances 2e⁻ ORR, their performance in acidic media is not as good as that in alkaline media as with the general trend of carbon materials. Fluorine, the element with the highest electronegativity, is powerful to alter the polarization and electronic structure of carbon for boosted H_2O_2 synthesis [135]. At pH of 1, F-doped hierarchically porous carbon with a fluorine content of 3.41 at% achieved the best H_2O_2 selectivity of 97.5% and production rate of 792.6 mmol h^{-1} g^{-1}. The CF_2 and CF_3 motifs are critical to 2e⁻ ORR by promoting O_2 activation and *OOH desorption.

4. Electrochemical device design and *in situ*/on-site utilization

4.1. Electrochemical device design

Alongside electrocatalyst design, developing well-configured electrochemical devices and reactors to perform bulk electrosynthesis of H_2O_2 is another important factor to achieve practical-scale application in this field. The design of real electrochemical devices should consider the mass transport of reactants and H_2O_2 disproportionation/decomposition during long-term electrolysis. In laboratory research, RRDE setup is typically used to quickly and quantitatively examine the H_2O_2 production on electrocatalysts (Fig. 8a) [14,28,141,142]. The Pt ring electrode should be electrochemically cleaned and refreshed before each use to make the H_2O_2 detection accurate [34,75]. However, because RRDE-based measurements are conducted under forced convection conditions in relatively short periods, it often fails to reflect the impact of mass transport limitation and long-term stability. In addition, the reported H_2O_2 selectivity by RRDE (molar fraction selectivity) is in most cases higher than the value reported at device level (Faradaic selectivity), which causes overestimation of catalyst performance [143]. The H-type cell is another widely used laboratory-scale cell configuration to accumulate H_2O_2 (Fig. 8b). In acidic electrolyte, the anode and cathode compartments are separated by a PEM to only allow H^+ transfer and avoid product crossover. Yamanaka et al. reported a series of H-type cell configurations to produce H_2O_2 in H_2/O_2 fuel cell and electrolyzer setups [144–147]. Using activated carbon and vapor-grown carbon fiber as cathode materials and a solid polymer electrolyte, the researchers synthesized neutral H_2O_2 solution of up to 8 wt% by electrolysis of water and oxygen [146]. Although H-type cells can simulate bulk electrosynthesis of H_2O_2, it is difficult to reach industrial-level current densities (e.g., > 100 mA cm^{-2}) and overcome the issue of mass transport limitation.

To facilitate O_2 diffusion at the cathode, many studies have turned to the gas diffusion electrode (GDE) comprising a porous and hydrophobic gas diffusion layer (GDL) and a catalyst layer (Fig. 8c) [148]. The electrocatalyst is deposited onto the catalyst layer to create a solid-liquid-gas triple-phase boundary. Mass transport of oxygen is significantly enhanced as its solubility in gas phase is greater than that in solution. Oxygen is continuously supplied to the cathode and the electrolyte containing H_2O_2 products is continuously drained away to regenerate catalytic active sites, thereby achieving large current density, high production rate and high H_2O_2 concentration simultaneously [149–151]. Since the produced H_2O_2 molecules need to transport through the GDL and catalyst layer to be collected in the electrolyte, the local H_2O_2 concentration near electrode surface can reach an excessive level for further reduction to water. Therefore, it is critical to control the continuous reactant and product circulation, which enables sufficient mass transport and prevents H_2O_2 accumulation. Li et al. developed a GDE-based H_2O_2 production system with a continuous flow of carrier water to remove the product, leading to a high H_2O_2 production rate of 200 μmol h^{-1} cm^{-2} without significant degradation of cobalt-carbon composite catalyst [152]. Considering that the as-produced H_2O_2 needs to be separated from the liquid electrolyte to obtain pure solutions, it is highly desirable to perform electrolyte-free H_2O_2 production to avoid further purification process [153]. Remarkably, Xia et al. achieved direct production of pure H_2O_2 solution in a solid-electrolyte H_2/O_2 fuel cell [154]. As shown in Fig. 8d, the electrogenerated H^+ and HO_2^- ions could transfer to the middle chamber and recombine to form H_2O_2 molecule in the porous solid electrolyte, which is then collected by pure deionized water. No ion contaminants are involved in this process, and a wide range of H_2O_2 concentration (up to 20 wt%) can be facilely and controllably acquired by tuning the water flow rate. This device achieved a high H_2O_2 selectivity > 90% and could retain performance after 100 hours.

Other types of reactors such as phase-transfer devices [155], jet reactors [156] and pressurized reactors [157–159] are also proposed for electrochemical H_2O_2 production. Murray et al. discovered that 2,7-disulfonyl anthraquinone ($AQDS^{2-}$) can catalyze 2e⁻ ORR and shuttle between aqueous and organic phases, which guides the design of phase-transfer H_2O_2 production devices (Fig. 8e) [155]. $AQDS^{2-}$ was first reduced to $AQDSH_2^{2-}$ by gaining two electrons, which subsequently performed phase-transfer between the aqueous electrolyte and organic phase, and finally was extracted from organic phase to form pure aqueous H_2O_2 solution. Continuous production of H_2O_2 at 2–3 μmol min^{-1} cm^{-2} with a concentration of 33 mM was achieved, highlighting the simultaneous generation and separation synthesis method. Generally, a permselective membrane is used between two electrode compartments, which however increases the ohmic resistance loss of the whole system and may become a limiting factor of stability. To this end, Chen et al. developed a membrane-free reactor with carbon catalysts, demonstrating a high H_2O_2 selectivity > 90% and an accumulated H_2O_2 concentration of 0.3 wt% (Fig. 8f) [160]. In the cathode compartment, oxygen is reduced to H_2O_2 and the GDE coated with hydrophobic polymer blocks the diffusion of H_2O_2, which enables the collection of concentrated H_2O_2 solution. Xia et al. also reported H_2O_2 production at both cathode and anode sides of a membrane-free cell with a high production rate of 24 μmol min^{-1} cm^{-2}) [151]. Because H_2O_2 can be generated by 2e⁻ oxygen reduction at the cathode and 2e⁻ water oxidation at the anode, the cell delivered an actual efficiency of 153%.

4.2. In situ and on-site application of electrosynthesized H_2O_2

Using intermittent and renewable electricity as an input, electrochemical 2e⁻ ORR enables the production of H_2O_2 in small amounts and flexible mode at the place and time of need. This method is especially suitable for decentralized and on-demand H_2O_2 production in remote areas, and avoids the cost and hazard associated with the handling of concentrated H_2O_2 solution. Along with electrocatalyst design and device engineering, the *in situ* application of electrosynthesized H_2O_2 from ORR is also an important determinant of scalability. Recent studies have shown the

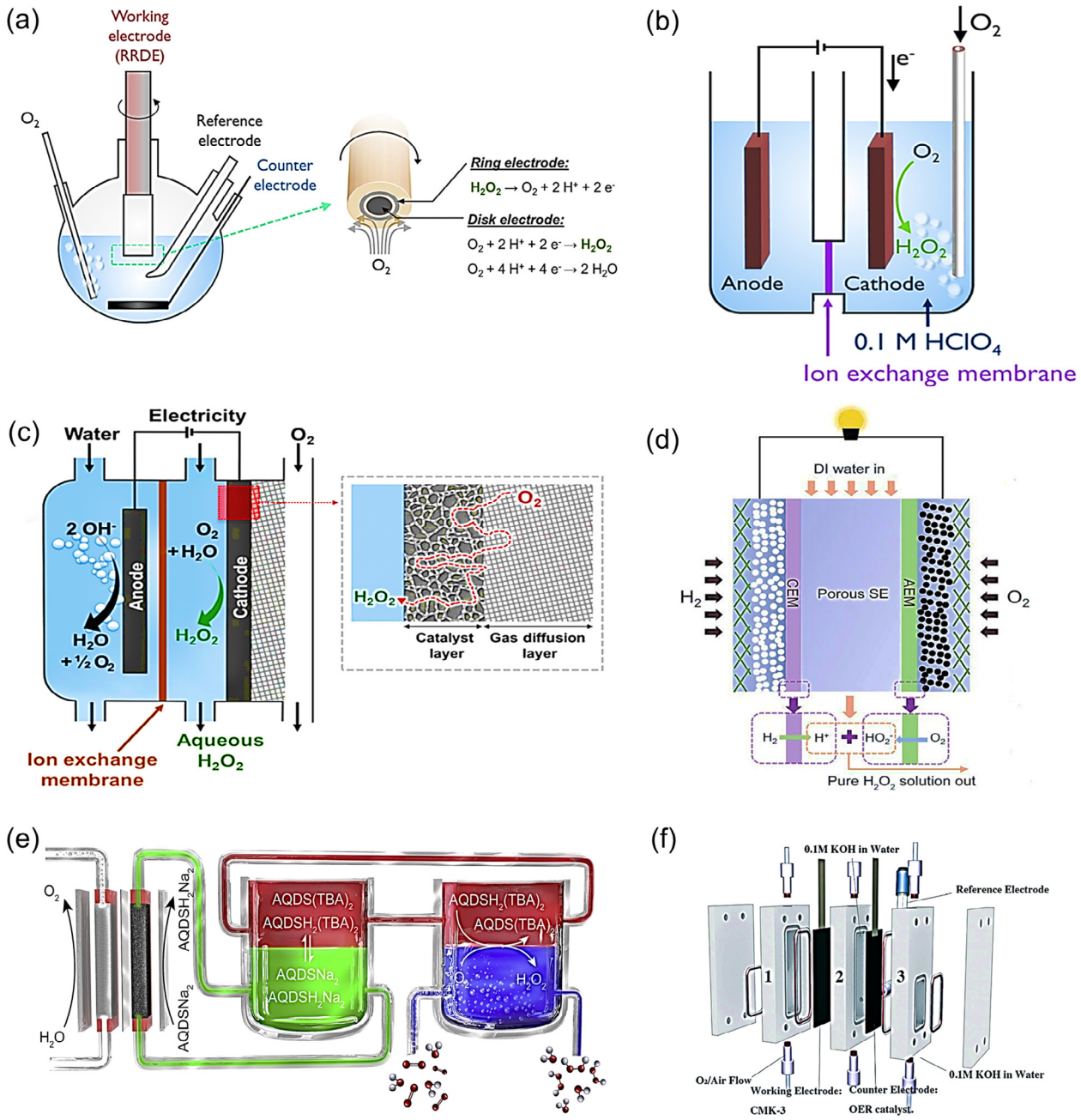

Fig. 8. Electrochemical device configurations for H_2O_2 synthesis. (a) RRDE setup and (b) H-type cell. (a and b) are reprinted from Ref. [14] with permission from the American Chemical Society. (c) Continuous flow cell by adopting a GDE. Reprinted from Ref. [148] with permission from the American Chemical Society. (d) Solid-electrolyte fuel cell. Reprinted from Ref. [154] with permission from AAAS. (e) Phase-transfer device. Reprinted from Ref. [155] with permission from Elsevier. (f) Membrane-free electrochemical H_2O_2 generator. Reprinted from Ref. [160] with permission from Royal Society of Chemistry.

potential applications of electrosynthesized H_2O_2 in a diverse range of fields, involving degradation of organic contaminants, disinfection and synthesis of value-added chemicals.

Large amounts of organic pollutants are released to wastewater and natural water bodies, which presents significant threats to human health and the environment [4]. The well-known electro-Fenton process is utilized as advanced oxidation process to convert organic contaminants into minerals, CO_2 and water. It features continuous electrocatalytic generation of Fenton reagents (Fe^{2+} and H_2O_2) and subsequent reaction to produce the strong oxidant hydroxyl radicals (·OH) [161–163]. Operating at the optimal pH range of 2.8–3.0, electro-Fenton system is able to treat organic dyes, pesticides, pharmaceuticals and other refractory compounds [4]. Dyes are present in wastewater from textile and printing industries, which would cause adverse effect on human health and present undesirable color. Electrocatalytic H_2O_2 generation on WO_3-modified Vulcan XC72 carbons showed 77% efficiency for Orange II decolorization as a result of *in situ* generated hydroxyl radicals [164]. Methylene blue [165], methyl orange [166], rhodamine B [110], acid red 14 [167] and acid orange [168] can also be degraded in a similar way. Electro-Fenton is also a powerful process to remove pesticides and pharmaceutical compounds. For example, Fe_3O_4@Fe_2O_3/activated carbon aerogel electrode exhibited 90% removal of imidacloprid within 30 min [169]. The out-

standing activity was facilitated by the high surface area (2410 m^2 g^{-1}) of activated carbon aerogel, whereas the dissolved Fe ions and surface Fe sites were responsible for the conversion of H_2O_2. Considering the fact that electro-Fenton system requires significant chemical and energy inputs, Xu et al. recently reported a combined H_2O_2 electrolyzer and Cu single-atom catalytic Fenton filter for organic wastewater treatment (Fig. 9a) [29]. Cu single atoms embedded in graphitic carbon nitride (C_3N_4) can activate H_2O_2 at pH of 7.0 to oxidize 50 μM rhodamine B within ~20 min and mineralize 95% of total organic carbon within 1 h. The use of Cu-C_3N_4 prevents catalyst leaching and does not affect effluent water quality. The designed organic wastewater treatment system can continuously produce 10 g L^{-1} H_2O_2 and completely oxidize triclosan, 17α-ethinyl oestradiol and cefazolin sodium to CO_2, thus demonstrating the significant potential of the whole system for organic removal.

The strong oxidation capacity of H_2O_2 makes it applicable for on-site and de-localized water disinfection. Wang group conducted a prototype experiment to examine the effectiveness of iron SACs with Fe-C-O motifs in neutral conditions (Fig. 9b) [30]. The achieved H_2O_2 selectivity maintained > 90% from 0.5 to 0.3 V vs RHE and the concentration reached 1613 ppm within 210 min electrolysis, corresponding to an average H_2O_2 Faradaic efficiency of 90.8%. The catalysts enabled > 99.9999% bacteria removal in 120 min at an electrode processing rate of 125 L h^{-1} m^{-2}. In addition, on-site generation of H_2O_2 from ORR for disinfection has been commercialized with some small-scale technological products available. For example, Lynntech, Inc. devised an electrochemical generator for H_2O_2 production under acidic conditions [170]. Using a GDE as cathode and platinized titanium as anode, the electrochemical cell can generate high-purity H_2O_2 solution of 6–7 wt% for use in disinfection directly or after proper dilution. HPNow, a Denmark-based technology and market leader of on-site electrochemical H_2O_2 generation, uses only air, water and electricity as inputs for safe, high-efficiency and scalable H_2O_2 synthesis [171]. A series of products based on the company's HPGen technology provide pure H_2O_2 solution of 1 to 5 kg per day, solving issues in agricultural, industrial and residential water treatment as well as sterilizing pathogens including COVID-19. Therefore, *in situ* and on-site H_2O_2 electrosynthesis is of great industrial interest as an environmentally friendly route for water disinfection.

Additionally, the as-generated H_2O_2 can be *in situ* integrated with subsequent oxidation reactions for synthesis of value-added chemicals [172,173]. In these reactions, the active species derived from H_2O_2 may include intermediates such as $\cdot HO_2$, $\cdot HO$ and HO_2^-, but their activities differ by 5–6 orders of magnitude [174]. As such, it is possible to perform selective organic oxidation to different extents and yield target products by regulating conditions. For example, electrogenerated H_2O_2 from 2e⁻ ORR is able to oxidize acetic acid to peroxyacetic acid of concentration up to 0.02 M on GDEs (Fig. 9c) [31,175]. Mechanistic study revealed that both H_2O_2 and *O species can react with acetic acid to form peroxyacetic

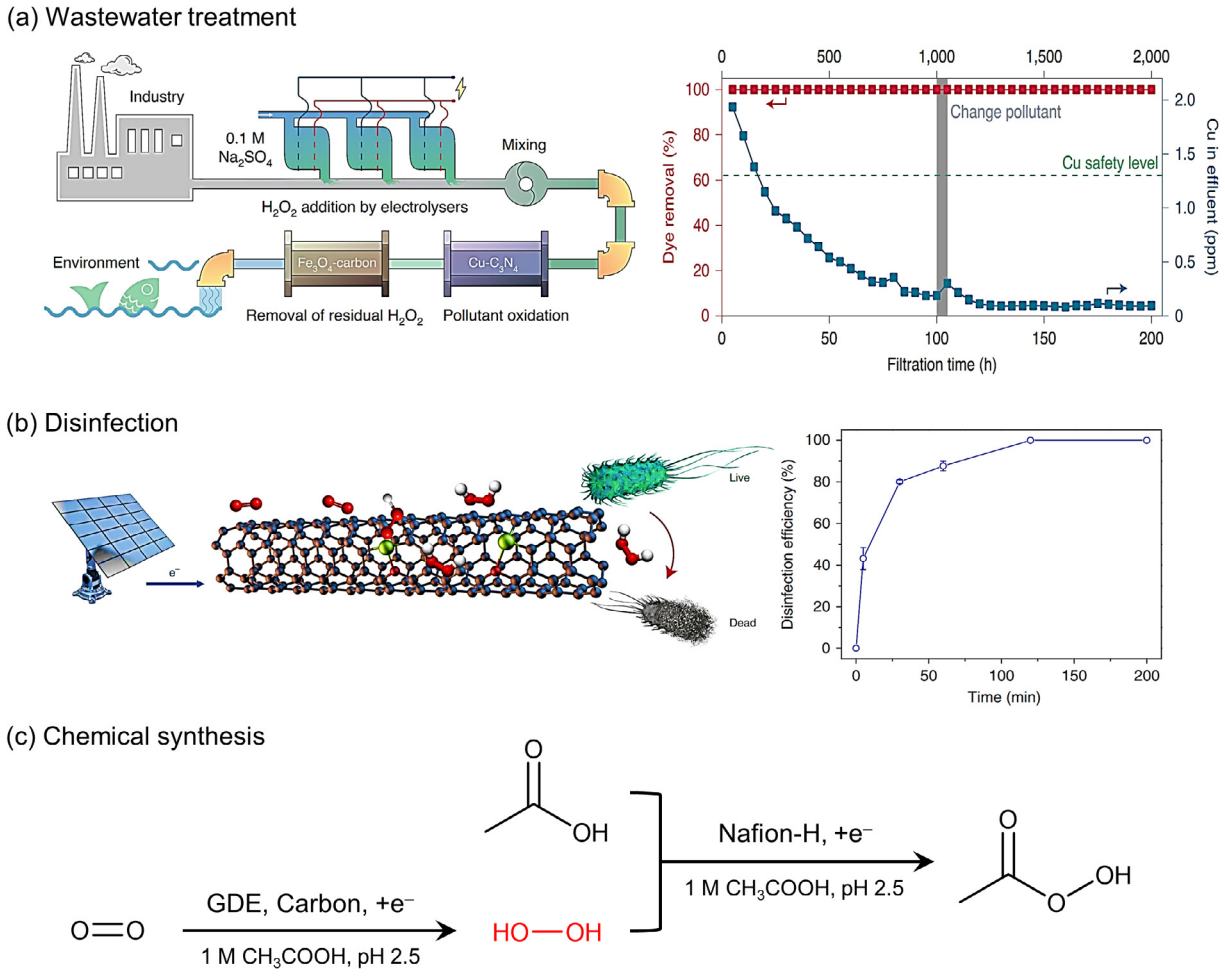

Fig. 9. Applications of electrosynthesized H_2O_2 from 2e⁻ ORR. (a) Organic wastewater treatment by *in situ* generated H_2O_2. Reprinted from Ref. [29] with permission from Springer Nature. (b) Bacteria killing and water disinfection by H_2O_2 produced on Fe-C-O SACs. Reprinted from Ref. [30] with permission from Springer Nature. (c) Synthesis of peroxyacetic acid by oxidation of acetic acid and *in situ* electrogenerated H_2O_2. Reprinted from Ref. [31] with permission from Elsevier.

acid, and H_2O_2 formation is the rate-limiting step. Such indirect electrochemical synthesis method is also applicable to the oxidation of n-butanol to n-butyric acid [176] and oxidation of olefinic compounds to corresponding epoxides [177]. More work remains to be done to uncover the reaction mechanism, especially the oxidation mechanism for the subsequent reaction, and the role of electrocatalysts in these tandem reactions [173].

5. Conclusions and perspectives

H_2O_2 plays a critical role in chemical industries and environmental remediation. Electrochemical H_2O_2 synthesis by $2e^-$ ORR offers a sustainable solution to on-site H_2O_2 production beyond traditional anthraquinone and direct synthesis approaches. The ability to produce H_2O_2 in acidic environment is of great importance, since acidic solutions of H_2O_2 is versatile in its most stable form and can fit in PEM devices. In this Review, we presented recent advances in electrochemical H_2O_2 production from $2e^-$ ORR in acid electrolytes, in terms of the pH effect on ORR mechanism, major types of electrocatalysts (Table 1), electrochemical devices, and potential applications. Despite significant advances, there are several aspects that need to be emphasized for further development of efficient H_2O_2 electrosynthesis in acidic solutions.

Firstly, elucidating the mechanism of $2e^-$ ORR and pH effect using advanced technologies is highly desired for catalyst development. Current CHE model-based DFT calculation works well in delineating the adsorption free energies of reaction intermediates, protons and electrons on the surface at constant potential [42]; however, it often oversimplifies a number of complex factors and has limitations in modelling the structure of electrode-electrolyte interface, the applied potential at operating conditions, surface charge effect and pH effect [178]. Therefore, it is urgent to develop more accurate models that consider these implicit factors, such as post-Hartree-Fock cluster calculations, embedding schemes, hybrid functionals and *operando* computations [61,179–181]. Moreover, with the advances in computer technologies and interdisciplinary research, machine learning has been applied in electrocatalysis for high-throughput catalyst screening that accelerates the discovery of new catalysts [182–184]. It is expected that future progress of machine learning algorithm will also help identify active catalysts and catalytic mechanisms of $2e^-$ ORR. In addition, for acidic H_2O_2 generation, a thorough understanding of pH effect is important but challenging. Most studies explore the pH dependency of $2e^-$ ORR by analyzing a specific material platform under different pH conditions, while the fundamental reasons behind the pH-dependent catalytic performance require further investigation.

Secondly, developing high-performance $2e^-$ ORR catalysts in acidic solutions is still an ongoing challenge. Practical application of electrochemical H_2O_2 production necessitates electrocatalysts with high ORR activity, high H_2O_2 selectivity, excellent stability, good electrical conductivity, facile mass transport and low cost. Unfortunately, no known materials satisfy all these criteria. Noble metals and their alloys exhibit the best activity and selectivity, but their scarcity and high cost largely hinder practical application. Synthesizing SACs is an effective way to maximize their atomic utilization efficiency, and their selectivity can be tuned to $2e^-$ route with favorable end-on adsorption of oxygen molecules. However, further explorations are needed to achieve high mass loading of metal atoms for maximized current density and resolve the complex structure–property relationship of SACs involving metal centers, first and second coordination spheres [34]. For metal-free materials, their ORR activity in acids is intrinsically lower than that in alkaline solutions. Thus, defect engineering, pore engineering and heteroatom doping are necessary to overcome the obstacles associated with the weak activation of O_2. Besides, present catalyst synthesis approaches inevitably generate carbon materials with heterogeneous surface features, leading to controversy over identifying the active sites. One possible remedy is to probe the surface chemistry under operating conditions by advanced *in situ* or *oper-*

Table 1
Performance of $2e^-$ ORR electrocatalysts in acidic media. $j_{0.1V}$ is disk current density at 0.1 V vs RHE estimated from LSV measurements with rotation speed of 1600 rpm unless otherwise specified. All potentials shown are versus RHE. PEMFC is Proton Exchange Membrane Fuel Cell.

Catalyst	Electrolyte	$j_{0.1V}$ (mA cm^{-2})	Selectivity (%@V)	Stability	Production rate (mmol g_{cat}^{-1} h^{-1}@V)	Reference
Noble-metal catalysts						
Pt-Hg	0.1 M $HClO_4$	3.6	~96@(0.2–0.4)	N/A	N/A	[35]
Pd-Hg/C	0.1 M $HClO_4$	N/A	>95@(0.35–0.55)	8,000 cycles	N/A	[21]
$Pd^{\delta+}$-OCNT	0.1 M $HClO_4$	2.0	95–98@(0.3–0.6)	>8h	1701@0.1 (H-cell)	[71]
PtP_2	0.1 M $HClO_4$	3.0	95–98.5@(0.1–0.4)	120 h	2825@0.4 (PEMFC)	[72]
Pt/HSC	0.1 M $HClO_4$	1.6@900 rpm	~95@(0.1–0.7)	2 h	48.75@0 (H-cell, 1 M $HClO_4$)	[77]
h-Pt_1-CuS_x	0.1 M $HClO_4$	2.7	92–96@(0.05–0.7)	10 h	546@0.05 (H-cell, 0.5 M $HClO_4$)	[81]
Non-noble-metal SACs						
Co-NC	0.1 M $HClO_4$	3.0	90–94@(0.3–0.6)	10 h	275@0.4 (H-cell)	[99]
Co-N-C	0.5 M H_2SO_4	3.0	75–80@(0.1–0.3)	4 h	90.9@0.1 (H-cell)	[47]
CoN_4 (O)	0.1 M $HClO_4$	3.0	>95@(0.3–0.6)	12 h	N/A	[107]
Co_1–NG(O)	0.1 M $HClO_4$	N/A	40–50@(0.2–0.7)	10 h	N/A	[100]
CoNOC	0.1 M $HClO_4$	2.8	>95@(0.1–0.6)	11 h	590@0.1 (H-cell)	[34]
Non-noble-metal compounds						
CoS_2	0.05 M H_2SO_4	2.0@2025 rpm	70–80@(0.2–0.7)	1 h	~24.5@0.5 (H-cell)	[109]
o-$CoSe_2$	0.05 M H_2SO_4	4.4@2025 rpm	~80@(0.5–0.7)	6 h	~15.2@0.5 (H-cell)	[110]
{001}-Fe_2O_{3-x}	5 mM H_2SO_4	1.2	90–100@(0.1–0.4)	~28 h	N/A	[115]
Metal-free catalysts						
MNC-50	0.5 M H_2SO_4	2.5	93–95@(0.1–0.3)	N/A	N/A	[125]
HPC-H24	0.05 M H_2SO_4 + 0.05 M Na_2SO_4 (pH 1)	2.7@1400 rpm	80–95@(−0.2–0.2)	2.5 h	294.0@0 (H-cell)	[124]
NCMK3IL50_800T	0.5 M H_2SO_4	1.7	95–98@(0.1–0.3)	6 h	159.9@0.1 (H-cell)	[128]
g-N-CNHs	0.1 M H_2SO_4	N/A	~80@0.2	24 h	N/A	[53]

ando characterizations to pinpoint the exact active motif. In all, there remains large room for improvement of H_2O_2 production performance in acidic media.

Lastly, research into electrochemical reactor design and *in situ*/on-site applications of H_2O_2 is as important as electrocatalyst design toward practical operation. The reported ORR performances are commonly based on half-cell test using RRDE setup, but relatively fewer reports test the catalysts in prototype or pilot-scale systems and achieve the standard of commercial viability. Efforts need to be devoted to the design of advanced electrochemical reactors, membranes and gas diffusion layers to obtain representative data under working conditions. Benchmarks of parameters, e.g., production rate, long-term durability, Faradaic efficiency and cost-effectiveness, also need to be established to allow meaningful performance comparison among different groups. Additionally, most applications of electrogenerated H_2O_2 are now based on the mature electro-Fenton process and take advantage of the strong oxidation capacity of ·OH, but the attack by reactive ·OH causes chemical degradation of PEMs and hinders the application in acidic media [185]. Hence, alternative technologies should be exploited to reach a diverse range of industrially relevant applications in chemical, energy and environmental fields. Moreover, the issue of energy input cannot be overlooked in practical application under large current densities. Ways to increase the energy conversion efficiency may be further explored for energy-saving decentralized H_2O_2 synthesis, for example by novel electricity and H_2O_2 co-generation systems [36] or pairing the anode side with $2e^-$ water oxidation to yield H_2O_2 with a theoretical Faradaic efficiency of 200%.

In short, we believe that the combined achievements of reaction mechanism, catalyst development, reactor engineering and on-site applications are necessary to accelerate the advancement of H_2O_2 electrosynthesis in acidic media. Overcoming the above-mentioned challenges will contribute to industrially relevant on-site H_2O_2 electrosynthesis performance, and laboratory-level research needs to be integrated closely with industries for promising commercialization. It is expected that the insights provided in this Review can also inspire developments of other electrocatalytic reactions for sustainable production of commodity chemicals, i.e. electrocatalytic refinery [173], eventually realizing a sustainable energy economy.

Declaration of Competing Interest

The authors declare that they have no known competing financial interests or personal relationships that could have appeared to influence the work reported in this paper.

Acknowledgments

C.T. acknowledges The University of Adelaide for Early Career Researcher Seed Funding (15128587). C.X. acknowledges the University of Electronic Science and Technology of China (UESTC) for Startup funding (A1098531023601264), and the National Natural Science Foundation of China (NSFC 22102018 and 52171201).

References

[1] R.L. Myers, The 100 Most Important Chemical Compounds: A Reference Guide, Greenwood Publishing Group, Westport, 2007.
[2] R. Ciriminna, L. Albanese, F. Meneguzzo, M. Pagliaro, ChemSusChem 9 (2016) 3374–3381.
[3] J.M. Campos-Martin, G. Blanco-Brieva, J.L. Fierro, Angew. Chem. Int. Ed. 45 (2006) 6962–6984.
[4] E. Brillas, I. Sires, M.A. Oturan, Chem. Rev. 109 (2009) 6570–6631.
[5] S.C. Perry, D. Pangotra, L. Vieira, L.-I. Csepei, V. Sieber, L. Wang, C. Ponce de León, F.C. Walsh, Nat. Rev. Chem. 3 (2019) 442–458.
[6] N. Wang, S. Ma, P. Zuo, J. Duan, B. Hou, Adv. Sci. 8 (2021) 2100076.
[7] J. Zhang, H. Zhang, M.J. Cheng, Q. Lu, Small 16 (2020) 1902845.
[8] United States Environmental Protection Agency, List N Advanced Search Page: Disinfectants for Coronavirus (COVID-19). https://www.epa.gov/coronavirus/list-n-advanced-search-page-disinfectants-coronavirus-covid-19/, 2021 (Accessed 29 September 2021).
[9] A.A. Caruso, A. Del Prete, A.I. Lazzarino, R. Capaldi, L. Grumetto, Infect. Control Hosp. Epidemiol. 41 (2020) 1360–1361.
[10] Y. Yi, L. Wang, G. Li, H. Guo, Catal. Sci. Technol. 6 (2016) 1593–1610.
[11] J.K. Edwards, B. Solsona, E.N. Ntainjua, A.F. Carley, A.A. Herzing, C.J. Kiely, G.J. Hutchings, Science 323 (2009) 1037–1041.
[12] J.K. Edwards, S.J. Freakley, R.J. Lewis, J.C. Pritchard, G.J. Hutchings, Catal. Today 248 (2015) 3–9.
[13] S.J. Freakley, Q. He, J.H. Harrhy, L. Lu, D.A. Crole, D.J. Morgan, E.N. Ntainjua, J.K. Edwards, A.F. Carley, A.Y. Borisevich, C.J. Kiely, G.J. Hutchings, Science 351 (2016) 965–968.
[14] S. Yang, A. Verdaguer-Casadevall, L. Arnarson, L. Silvioli, V. Čolić, R. Frydendal, J. Rossmeisl, I. Chorkendorff, I.E.L. Stephens, ACS Catal. 8 (2018) 4064–4081.
[15] Y. Jiang, P. Ni, C. Chen, Y. Lu, P. Yang, B. Kong, A. Fisher, X. Wang, Adv. Energy Mater. 8 (2018) 1801909.
[16] M. Melchionna, P. Fornasiero, M. Prato, Adv. Mater. 31 (2019) 1802920.
[17] K. Jiang, J. Zhao, H. Wang, Adv. Funct. Mater. 30 (2020) 2003321.
[18] H. Jin, C. Guo, X. Liu, J. Liu, A. Vasileff, Y. Jiao, Y. Zheng, S.-Z. Qiao, Chem. Rev. 118 (2018) 6337–6408.
[19] B.-Q. Li, C.-X. Zhao, J.-N. Liu, Q. Zhang, Adv. Mater. 31 (2019) 1808173.
[20] S. Siahrostami, S.J. Villegas, A.H.B. Mostaghimi, S. Back, A.B. Farimani, H. Wang, K.A. Persson, J. Montoya, ACS Catal. 10 (2020) 7495–7511.
[21] A. Verdaguer-Casadevall, D. Deiana, M. Karamad, S. Siahrostami, P. Malacrida, T.W. Hansen, J. Rossmeisl, I. Chorkendorff, I.E.L. Stephens, Nano Lett. 14 (2014) 1603–1608.
[22] J. Gao, B. Liu, ACS Materials Lett. 2 (2020) 1008–1024.
[23] Z. Qiang, J.H. Chang, C.P. Huang, Water Res. 36 (2002) 85–94.
[24] A. Kulkarni, S. Siahrostami, A. Patel, J.K. Nørskov, Chem. Rev. 118 (2018) 2302–2312.
[25] Y. Pang, H. Xie, Y. Sun, M.-M. Titirici, G.-L. Chai, J. Mater. Chem. A 8 (2020) 24996–25016.
[26] E. Berl, Trans. Electrochem. Soc. 76 (1939) 359–369.
[27] X. Zhang, Y. Xia, C. Xia, H. Wang, Trends Chem. 2 (2020) 942–953.
[28] J. Tang, T. Zhao, D. Solanki, X. Miao, W. Zhou, S. Hu, Joule 5 (2021) 1432–1461.
[29] J. Xu, X. Zheng, Z. Feng, Z. Lu, Z. Zhang, W. Huang, Y. Li, D. Vuckovic, Y. Li, S. Dai, G. Chen, K. Wang, H. Wang, J.K. Chen, W. Mitch, Y. Cui, Nat. Sustain. 4 (2021) 233–241.
[30] K. Jiang, S. Back, A.J. Akey, C. Xia, Y. Hu, W. Liang, D. Schaak, E. Stavitski, J.K. Nørskov, S. Siahrostami, H. Wang, Nat. Commun. 10 (2019) 3997.
[31] M.S. Saha, A. Denggerile, Y. Nishiki, T. Furuta, T. Ohsaka, Electrochem. Commun. 5 (2003) 445–448.
[32] Y. Jiao, Y. Zheng, M. Jaroniec, S.Z. Qiao, J. Am. Chem. Soc. 136 (2014) 4394–4403.
[33] X.-R. Wang, J.-Y. Liu, Z.-W. Liu, W.-C. Wang, J. Luo, X.-P. Han, X.-W. Du, S.-Z. Qiao, J. Yang, Adv. Mater. 30 (2018) 1800005.
[34] C. Tang, L. Chen, H. Li, L. Li, Y. Jiao, Y. Zheng, H. Xu, K. Davey, S.-Z. Qiao, J. Am. Chem. Soc. 143 (2021) 7819–7827.
[35] S. Siahrostami, A. Verdaguer-Casadevall, M. Karamad, D. Deiana, P. Malacrida, B. Wickman, M. Escudero-Escribano, E.A. Paoli, R. Frydendal, T.W. Hansen, I. Chorkendorff, I.E.L. Stephens, J. Rossmeisl, Nat. Mater. 12 (2013) 1137–1143.
[36] K. Wang, J. Huang, H. Chen, Y. Wang, S. Song, Chem. Commun. 56 (2020) 12109–12121.
[37] E. Watanabe, H. Ushiyama, K. Yamashita, Catal. Sci. Technol. 5 (2015) 2769–2776.
[38] J. Cheng, F. Libisch, E.A. Carter, J. Phys. Chem. Lett. 6 (2015) 1661–1665.
[39] M.M. Montemore, M.A. van Spronsen, R.J. Madix, C.M. Friend, Chem. Rev. 118 (2018) 2816–2862.
[40] V. Viswanathan, H.A. Hansen, J. Rossmeisl, J.K. Nørskov, J. Phys. Chem. Lett. 3 (2012) 2948–2951.
[41] A.S. Bandarenka, H.A. Hansen, J. Rossmeisl, I.E.L. Stephens, Phys. Chem. Chem. Phys. 16 (2014) 13625–13629.
[42] J.K. Nørskov, J. Rossmeisl, A. Logadottir, L. Lindqvist, J.R. Kitchin, T. Bligaard, H. Jónsson, J. Phys. Chem. B 108 (2004) 17886–17892.
[43] V. Viswanathan, H.A. Hansen, J. Rossmeisl, J.K. Nørskov, ACS Catal. 2 (2012) 1654–1660.
[44] Z.W. Seh, J. Kibsgaard, C.F. Dickens, I. Chorkendorff, J.K. Nørskov, T.F. Jaramillo, Science 355 (2017) eaad4998.
[45] N. Ramaswamy, S. Mukerjee, J. Phys. Chem. C 115 (2011) 18015–18026.
[46] S. Rojas-Carbonell, K. Artyushkova, A. Serov, C. Santoro, I. Matanovic, P. Atanassov, ACS Catal. 8 (2018) 3041–3053.
[47] Y. Sun, L. Silvioli, N.R. Sahraie, W. Ju, J. Li, A. Zitolo, S. Li, A. Bagger, L. Arnarson, X. Wang, T. Moeller, D. Bernsmeier, J. Rossmeisl, F. Jaouen, P. Strasser, J. Am. Chem. Soc. 141 (2019) 12372–12381.
[48] D. San Roman, D. Krishnamurthy, R. Garg, H. Hafiz, M. Lamparski, N.T. Nuhfer, V. Meunier, V. Viswanathan, T. Cohen-Karni, ACS Catal. 10 (2020) 1993–2008.
[49] Y.J. Sa, J.H. Kim, S.H. Joo, Angew. Chem. Int. Ed. 58 (2019) 1100–1105.
[50] S. Chen, Z. Chen, S. Siahrostami, T.R. Kim, D. Nordlund, D. Sokaras, S. Nowak, J. W.F. To, D. Higgins, R. Sinclair, J.K. Nørskov, T.F. Jaramillo, Z. Bao, ACS Sustainable Chem. Eng. 6 (2017) 311–317.
[51] Z. Lu, G. Chen, S. Siahrostami, Z. Chen, K. Liu, J. Xie, L. Liao, T. Wu, D. Lin, Y. Liu, T.F. Jaramillo, J.K. Nørskov, Y. Cui, Nat. Catal. 1 (2018) 156–162.

[52] H.W. Kim, M.B. Ross, N. Kornienko, L. Zhang, J. Guo, P. Yang, B.D. McCloskey, Nat. Catal. 1 (2018) 282–290.
[53] D. Iglesias, A. Giuliani, M. Melchionna, S. Marchesan, A. Criado, L. Nasi, M. Bevilacqua, C. Tavagnacco, F. Vizza, M. Prato, P. Fornasiero, Chem 4 (2018) 106–123.
[54] L. Li, C. Tang, Y. Zheng, B. Xia, X. Zhou, H. Xu, S.-Z. Qiao, Adv. Energy Mater. 10 (2020) 2000789.
[55] Y.-H. Lee, F. Li, K.-H. Chang, C.-C. Hu, T. Ohsaka, Appl. Catal. B 126 (2012) 208–214.
[56] Y. Xia, X. Zhao, C. Xia, Z.-Y. Wu, P. Zhu, J.Y.T. Kim, X. Bai, G. Gao, Y. Hu, J. Zhong, Y. Liu, H. Wang, Nat. Commun. 12 (2021) 4225.
[57] S. Chen, Z. Chen, S. Siahrostami, D. Higgins, D. Nordlund, D. Sokaras, T.R. Kim, Y. Liu, X. Yan, E. Nilsson, R. Sinclair, J.K. Nørskov, T.F. Jaramillo, Z. Bao, J. Am. Chem. Soc. 140 (2018) 7851–7859.
[58] F. Hasché, M. Oezaslan, P. Strasser, T.-P. Fellinger, J. Energy Chem. 25 (2016) 251–257.
[59] B.W. Noffke, Q. Li, K. Raghavachari, L. Li, J. Am. Chem. Soc. 138 (2016) 13923–13929.
[60] G.-L. Chai, Z. Hou, T. Ikeda, K. Terakura, J. Phys. Chem. C 121 (2017) 14524–14533.
[61] X. Zhao, Y. Liu, J. Am. Chem. Soc. 143 (2021) 9423–9428.
[62] C.H. Choi, H.C. Kwon, S. Yook, H. Shin, H. Kim, M. Choi, J. Phys. Chem. C 118 (2014) 30063–30070.
[63] Y.L. Wang, S. Gurses, N. Felvey, A. Boubnov, S.S. Mao, C.X. Kronawitter, ACS Catal. 9 (2019) 8453–8463.
[64] G.V. Fortunato, E. Pizzutilo, A.M. Mingers, O. Kasian, S. Cherevko, E.S.F. Cardoso, K.J.J. Mayrhofer, G. Maia, M. Ledendecker, J. Phys. Chem. C 122 (2018) 15878–15885.
[65] J.S. Jirkovský, M. Halasa, D.J. Schiffrin, Phys. Chem. Chem. Phys. 12 (2010) 8042–8052.
[66] Y. Lu, Y. Jiang, X. Gao, W. Chen, Chem. Commun. 50 (2014) 8464–8467.
[67] E. Pizzutilo, O. Kasian, C.H. Choi, S. Cherevko, G.J. Hutchings, K.J.J. Mayrhofer, S.J. Freakley, Chem. Phys. Lett. 683 (2017) 436–442.
[68] E. Pizzutilo, S.J. Freakley, S. Cherevko, S. Venkatesan, G.J. Hutchings, C.H. Liebscher, G. Dehm, K.J.J. Mayrhofer, ACS Catal. 7 (2017) 5699–5705.
[69] X. Zhao, H. Yang, J. Xu, T. Cheng, Y. Li, ACS Materials Lett. 3 (2021) 996–1002.
[70] Q. Shi, W. Zhu, H. Zhong, C. Zhu, H. Tian, J. Li, M. Xu, D. Su, X. Li, D. Liu, B.Z. Xu, S.P. Beckman, D. Du, Y. Lin, ACS Appl. Energy Mater. 2 (2019) 7722–7727.
[71] Q. Chang, P. Zhang, A.H.B. Mostaghimi, X. Zhao, S.R. Denny, J.H. Lee, H. Gao, Y. Zhang, H.L. Xin, S. Siahrostami, J.G. Chen, Z. Chen, Nat. Commun. 11 (2020) 2178.
[72] H. Li, P. Wen, D.S. Itanze, Z.D. Hood, S. Adhikari, C. Lu, X. Ma, C. Dun, L. Jiang, D. L. Carroll, Y. Qiu, S.M. Geyer, Nat. Commun. 11 (2020) 3928.
[73] C. Yang, S. Bai, Z. Yu, Y. Feng, B. Huang, Q. Lu, T. Wu, M. Sun, T. Zhu, C. Cheng, L. Zhang, Q. Shao, X. Huang, Nano Energy 89 (2021) 106480.
[74] A. Wang, J. Li, T. Zhang, Nat. Rev. Chem. 2 (2018) 65–81.
[75] C. Tang, Y. Jiao, B. Shi, J.-N. Liu, Z. Xie, X. Chen, Q. Zhang, S.-Z. Qiao, Angew. Chem. Int. Ed. 59 (2020) 9171–9176.
[76] S. Yang, J. Kim, Y.J. Tak, A. Soon, H. Lee, Angew. Chem. Int. Ed. 55 (2016) 2058–2062.
[77] C.H. Choi, M. Kim, H.C. Kwon, S.J. Cho, S. Yun, H.-T. Kim, K.J.J. Mayrhofer, H. Kim, M. Choi, Nat. Commun. 7 (2016) 10922.
[78] J. Kim, H.-E. Kim, H. Lee, ChemSusChem 11 (2018) 104–113.
[79] I. Katsounaros, W.B. Schneider, J.C. Meier, U. Benedikt, P.U. Biedermann, A.A. Auer, K.J.J. Mayrhofer, Phys. Chem. Chem. Phys. 14 (2012) 7384–7391.
[80] S. Yang, Y.J. Tak, J. Kim, A. Soon, H. Lee, ACS Catal. 7 (2017) 1301–1307.
[81] R. Shen, W. Chen, Q. Peng, S. Lu, L. Zheng, X. Cao, Y. Wang, W. Zhu, J. Zhang, Z. Zhuang, C. Chen, D. Wang, Y. Li, Chem 5 (2019) 2099–2110.
[82] S.K. Sahoo, Y. Ye, S. Lee, J. Park, H. Lee, J. Lee, J.W. Han, ACS Energy Lett. 4 (2018) 126–132.
[83] J.S. Jirkovský, I. Panas, E. Ahlberg, M. Halasa, S. Romani, D.J. Schiffrin, J. Am. Chem. Soc. 133 (2011) 19432–19441.
[84] H.-E. Kim, I.H. Lee, J. Cho, S. Shin, H.C. Ham, J.Y. Kim, H. Lee, ChemElectroChem 6 (2019) 4757–4764.
[85] Z. Wei, B. Deng, P. Chen, T. Zhao, S. Zhao, Chem. Eng. J. 428 (2022) 131112.
[86] M. Ledendecker, E. Pizzutilo, G. Malta, G.V. Fortunato, K.J.J. Mayrhofer, G.J. Hutchings, S.J. Freakley, ACS Catal. 10 (2020) 5928–5938.
[87] J.H. Kim, D. Shin, J. Lee, D.S. Baek, T.J. Shin, Y.-T. Kim, H.Y. Jeong, J.H. Kwak, H. Kim, S.H. Joo, ACS Nano 14 (2020) 1990–2001.
[88] Y. Chen, S. Ji, C. Chen, Q. Peng, D. Wang, Y. Li, Joule 2 (2018) 1242–1264.
[89] H. Zhang, G. Liu, L. Shi, J. Ye, Adv. Energy Mater. 8 (2018) 1701343.
[90] W. Liu, H. Zhang, C. Li, X. Wang, J. Liu, X. Zhang, J. Energy Chem. 47 (2020) 333–345.
[91] L. Yang, D. Cheng, H. Xu, X. Zeng, X. Wan, J. Shui, Z. Xiang, D. Cao, Proc. Natl. Acad. Sci. U. S. A. 115 (2018) 6626–6631.
[92] J. Li, S. Chen, N. Yang, M. Deng, S. Ibraheem, J. Deng, J. Li, L. Li, Z. Wei, Angew. Chem. Int. Ed. 58 (2019) 7035–7039.
[93] H. Fei, J. Dong, Y. Feng, C.S. Allen, C. Wan, B. Volosskiy, M. Li, Z. Zhao, Y. Wang, H. Sun, P. An, W. Chen, Z. Guo, C. Lee, D. Chen, I. Shakir, M. Liu, T. Hu, Y. Li, A.I. Kirkland, X. Duan, Y. Huang, Nat. Catal. 1 (2018) 63–72.
[94] L. Li, B. Huang, X. Tang, Y. Hong, W. Zhai, T. Hu, K. Yuan, Y. Chen, Adv. Funct. Mater. 31 (2021) 2103857.
[95] X.X. Wang, D.A. Cullen, Y.-T. Pan, S. Hwang, M. Wang, Z. Feng, J. Wang, M.H. Engelhard, H. Zhang, Y. He, Y. Shao, D. Su, K.L. More, J.S. Spendelow, G. Wu, Adv. Mater. 30 (2018) 1706758.
[96] Y. He, H. Guo, S. Hwang, X. Yang, Z. He, J. Braaten, S. Karakalos, W. Shan, M. Wang, H. Zhou, Z. Feng, K.L. More, G. Wang, D. Su, D.A. Cullen, L. Fei, S. Litster, G. Wu, Adv. Mater. 32 (2020) 2003577.
[97] C. Zhu, Q. Shi, B.Z. Xu, S. Fu, G. Wan, C. Yang, S. Yao, J. Song, H. Zhou, D. Du, S.P. Beckman, D. Su, Y. Lin, Adv. Energy Mater. 8 (2018) 1801956.
[98] X. Xie, C. He, B. Li, Y. He, D.A. Cullen, E.C. Wegener, A.J. Kropf, U. Martinez, Y. Cheng, M.H. Engelhard, M.E. Bowden, M. Song, T. Lemmon, X.S. Li, Z. Nie, J. Liu, D.J. Myers, P. Zelenay, G. Wang, G. Wu, V. Ramani, Y. Shao, Nat. Catal. 3 (2020) 1044–1054.
[99] J. Gao, H.B. Yang, X. Huang, S.-F. Hung, W. Cai, C. Jia, S. Miao, H.M. Chen, X. Yang, Y. Huang, T. Zhang, B. Liu, Chem 6 (2020) 658–674.
[100] E. Jung, H. Shin, B.-H. Lee, V. Efremov, S. Lee, H.S. Lee, J. Kim, W. Hooch Antink, S. Park, K.-S. Lee, S.-P. Cho, J.S. Yoo, Y.-E. Sung, T. Hyeon, Nat. Mater. 19 (2020) 436–442.
[101] C. Zhao, C. Xiong, X. Liu, M. Qiao, Z. Li, T. Yuan, J. Wang, Y. Qu, X. Wang, F. Zhou, Q. Xu, S. Wang, M. Chen, W. Wang, Y. Li, T. Yao, Y. Wu, Y. Li, Chem. Commun. 55 (2019) 2285–2288.
[102] L. Jiao, H. Yan, Y. Wu, W. Gu, C. Zhu, D. Du, Y. Lin, Angew. Chem. Int. Ed. 59 (2020) 2565–2576.
[103] P. Gotico, B. Boitrel, R. Guillot, M. Sircoglou, A. Quaranta, Z. Halime, W. Leibl, A. Aukauloo, Angew. Chem. Int. Ed. 58 (2019) 4504–4509.
[104] C.-X. Zhao, B.-Q. Li, J.-N. Liu, Q. Zhang, Angew. Chem. Int. Ed. 60 (2021) 4448–4463.
[105] D. Liu, Q. He, S. Ding, L. Song, Adv. Energy Mater. 10 (2020) 2001482.
[106] C. Liu, H. Li, F. Liu, J. Chen, Z. Yu, Z. Yuan, C. Wang, H. Zheng, G. Henkelman, L. Wei, Y. Chen, J. Am. Chem. Soc. 142 (2020) 21861–21871.
[107] Q. Zhang, X. Tan, N.M. Bedford, Z. Han, L. Thomsen, S. Smith, R. Amal, X. Lu, Nat. Commun. 11 (2020) 4181.
[108] J.S. Jirkovský, A. Björling, E. Ahlberg, J. Phys. Chem. C 116 (2012) 24436–24444.
[109] H. Sheng, E.D. Hermes, X. Yang, D. Ying, A.N. Janes, W. Li, J.R. Schmidt, S. Jin, ACS Catal. 9 (2019) 8433–8442.
[110] H. Sheng, A.N. Janes, R.D. Ross, D. Kaiman, J. Huang, B. Song, J.R. Schmidt, S. Jin, Energy Environ. Sci. 13 (2020) 4189–4203.
[111] X. Zhao, Y. Wang, Y. Da, X. Wang, T. Wang, M. Xu, X. He, W. Zhou, Y. Li, J.N. Coleman, Y. Li, Natl. Sci. Rev. 7 (2020) 1360–1366.
[112] J. Liang, Y. Wang, Q. Liu, Y. Luo, T. Li, H. Zhao, S. Lu, F. Zhang, A.M. Asiri, F. Liu, D. Ma, X. Sun, J. Mater. Chem. A 9 (2021) 6117–6122.
[113] L. Zhang, J. Liang, L. Yue, Z. Xu, K. Dong, Q. Liu, Y. Luo, T. Li, X. Cheng, G. Cui, B. Tang, A.A. Alshehri, K.A. Alzahrani, X. Guo, X. Sun, Nano Res. DOI: 10.1007/s12274-021-3474-0.
[114] J.F. Carneiro, M.J. Paulo, M. Siaj, A.C. Tavares, M.R.V. Lanza, J. Catal. 332 (2015) 51–61.
[115] R. Gao, L. Pan, Z. Li, C. Shi, Y. Yao, X. Zhang, J.-J. Zou, Adv. Funct. Mater. 30 (2020) 1910539.
[116] J.F. Carneiro, M.J. Paulo, M. Siaj, A.C. Tavares, M.R.V. Lanza, ChemElectroChem 4 (2017) 508–513.
[117] X. Huang, P. Oleynikov, H. He, A. Mayoral, L. Mu, F. Lin, Y.B. Zhang, Nano Res. DOI: 10.1007/s12274-021-3382-3.
[118] A. Byeon, J. Cho, J.M. Kim, K.H. Chae, H.-Y. Park, S.W. Hong, H.C. Ham, S.W. Lee, K.R. Yoon, J.Y. Kim, Nanoscale Horiz. 5 (2020) 832–838.
[119] A. Lenarda, M. Bevilacqua, C. Tavagnacco, L. Nasi, A. Criado, F. Vizza, M. Melchionna, M. Prato, P. Fornasiero, ChemSusChem 12 (2019) 1664–1672.
[120] M. Campos, W. Siriwatcharapiboon, R.J. Potter, S.L. Horswell, Catal. Today 202 (2013) 135–143.
[121] R.M. Reis, R.B. Valim, R.S. Rocha, A.S. Lima, P.S. Castro, M. Bertotti, M.R.V. Lanza, Electrochim. Acta 139 (2014) 1–6.
[122] Y.P. Zhu, C. Guo, Y. Zheng, S.-Z. Qiao, Acc. Chem. Res. 50 (2017) 915–923.
[123] K. Gong, F. Du, Z. Xia, M. Durstock, L. Dai, Science 323 (2009) 760–764.
[124] Y. Liu, X. Quan, X. Fan, H. Wang, S. Chen, Angew. Chem. Int. Ed. 54 (2015) 6837–6841.
[125] J. Park, Y. Nabae, T. Hayakawa, M. Kakimoto, ACS Catal. 4 (2014) 3749–3754.
[126] D. Yan, Y. Li, J. Huo, R. Chen, L. Dai, S. Wang, Adv. Mater. 29 (2017) 1606459.
[127] C. Tang, Q. Zhang, Adv. Mater. 29 (2017) 1604103.
[128] Y. Sun, I. Sinev, W. Ju, A. Bergmann, S. Dresp, S. Kühl, C. Spöri, H. Schmies, H. Wang, D. Bernsmeier, B. Paul, R. Schmack, R. Kraehnert, B.R. Cuenya, P. Strasser, ACS Catal. 8 (2018) 2844–2856.
[129] V. Čolić, S. Yang, Z. Révay, I.E.L. Stephens, I. Chorkendorff, Electrochim. Acta 272 (2018) 192–202.
[130] L. Jing, C. Tang, Q. Tian, T. Liu, S. Ye, P. Su, Y. Zheng, J. Liu, ACS Appl. Mater. Interfaces 13 (2021) 39763–39771.
[131] Y. Wu, A. Muthukrishnan, S. Nagata, Y. Nabae, J. Phys. Chem. C 123 (2019) 4590–4596.
[132] T.-P. Fellinger, F. Hasché, P. Strasser, M. Antonietti, J. Am. Chem. Soc. 134 (2012) 4072–4075.
[133] Y. Sun, S. Li, Z.P. Jovanov, D. Bernsmeier, H. Wang, B. Paul, X. Wang, S. Kuhl, P. Strasser, ChemSusChem 11 (2018) 3388–3395.
[134] D. Guo, R. Shibuya, C. Akiba, S. Saji, T. Kondo, J. Nakamura, Science 351 (2016) 361–365.
[135] K. Zhao, Y. Su, X. Quan, Y. Liu, S. Chen, H. Yu, J. Catal. 357 (2018) 118–126.
[136] G.-F. Han, F. Li, W. Zou, M. Karamad, J.-P. Jeon, S.-W. Kim, S.-J. Kim, Y. Bu, Z. Fu, Y. Lu, S. Siahrostami, J.-B. Baek, Nat. Commun. 11 (2020) 2209.
[137] N. Jia, T. Yang, S. Shi, X. Chen, Z. An, Y. Chen, S. Yin, P. Chen, ACS Sustainable Chem. Eng. 8 (2020) 2883–2891.
[138] V. Perazzolo, G. Daniel, R. Brandiele, L. Picelli, G.A. Rizzi, A.A. Isse, C. Durante, Chem. Eur. J. 27 (2021) 1002–1014.

[139] Y. Zhang, M. Melchionna, M. Medved, P. Błoński, T. Steklý, A. Bakandritsos, Š. Kment, R. Zbořil, M. Otyepka, P. Fornaserio, A. Naldoni, ChemCatChem 13 (2021) 4372–4383.
[140] V. Perazzolo, C. Durante, R. Pilot, A. Paduano, J. Zheng, G.A. Rizzi, A. Martucci, G. Granozzi, A. Gennaro, Carbon 95 (2015) 949–963.
[141] T.J. Schmidt, H.A. Gasteiger, G.D. Stäb, P.M. Urban, D.M. Kolb, R.J. Behm, J. Electrochem. Soc. 145 (1998) 2354–2358.
[142] R. Zhou, Y. Zheng, M. Jaroniec, S.-Z. Qiao, ACS Catal. 6 (2016) 4720–4728.
[143] C. Xia, J.Y. Kim, H. Wang, Nat. Catal. 3 (2020) 605–607.
[144] I. Yamanaka, T. Hashimoto, K. Otsuka, Chem. Lett. 31 (2002) 852–853.
[145] I. Yamanaka, T. Onizawa, S. Takenaka, K. Otsuka, Angew. Chem. Int. Ed. 42 (2003) 3653–3655.
[146] I. Yamanaka, T. Murayama, Angew. Chem. Int. Ed. 47 (2008) 1900–1902.
[147] I. Yamanaka, S. Tazawa, T. Murayama, R. Ichihashi, N. Hanaizumi, ChemSusChem 1 (2008) 988–992.
[148] E. Jung, H. Shin, W. Hooch Antink, Y.-E. Sung, T. Hyeon, ACS Energy Lett 5 (2020) 1881–1892.
[149] S. Ren, D. Joulié, D. Salvatore, K. Torbensen, M. Wang, M. Robert, C.P. Berlinguette, Science 365 (2019) 367–369.
[150] T. Burdyny, W.A. Smith, Energy Environ. Sci. 12 (2019) 1442–1453.
[151] C. Xia, S. Back, S. Ringe, K. Jiang, F. Chen, X. Sun, S. Siahrostami, K. Chan, H. Wang, Nat. Catal. 3 (2020) 125–134.
[152] W. Li, A. Bonakdarpour, E. Gyenge, D.P. Wilkinson, ChemSusChem 6 (2013) 2137–2143.
[153] T.H. Jeon, B. Kim, C. Kim, C. Xia, H. Wang, P.J.J. Alvarez, W. Choi, Energy Environ. Sci. 14 (2021) 3110–3119.
[154] C. Xia, Y. Xia, P. Zhu, L. Fan, H. Wang, Science 366 (2019) 226–231.
[155] A.T. Murray, S. Voskian, M. Schreier, T.A. Hatton, Y. Surendranath, Joule 3 (2019) 2942–2954.
[156] J.F. Pérez, J. Llanos, C. Sáez, C. López, P. Cañizares, M.A. Rodrigo, Electrochem. Commun. 71 (2016) 65–68.
[157] O. Scialdone, A. Galia, C. Gattuso, S. Sabatino, B. Schiavo, Electrochim. Acta 182 (2015) 775–780.
[158] J.F. Pérez, A. Galia, M.A. Rodrigo, J. Llanos, S. Sabatino, C. Sáez, B. Schiavo, O. Scialdone, Electrochim. Acta 248 (2017) 169–177.
[159] J.F. Pérez, S. Sabatino, A. Galia, M.A. Rodrigo, J. Llanos, C. Sáez, O. Scialdone, Electrochim. Acta 273 (2018) 447–453.
[160] Z. Chen, S. Chen, S. Siahrostami, P. Chakthranont, C. Hahn, D. Nordlund, S. Dimosthenis, J.K. Nørskov, Z. Bao, T.F. Jaramillo, React, Chem. Eng. 2 (2017) 239–245.
[161] E. Brillas, E. Mur, J. Casado, J. Electrochem. Soc. 143 (1996) L49–L53.
[162] M.A. Oturan, J. Peiroten, P. Chartrin, A.J. Acher, Environ. Sci. Technol. 34 (2000) 3474–3479.
[163] H.Y. Zhao, L. Qian, Y. Chen, Q.N. Wang, G.H. Zhao, Chem. Eng. J. 332 (2018) 486–498.
[164] E.C. Paz, L.R. Aveiro, V.S. Pinheiro, F.M. Souza, V.B. Lima, F.L. Silva, P. Hammer, M.R.V. Lanza, M.C. Santos, Appl. Catal. B 232 (2018) 436–445.
[165] C.-Y. Chen, C. Tang, H.-F. Wang, C.-M. Chen, X. Zhang, X. Huang, Q. Zhang, ChemSusChem 9 (2016) 1194–1199.
[166] F. Yu, M. Zhou, X. Yu, Electrochim. Acta 163 (2015) 182–189.
[167] A. Wang, J. Qu, J. Ru, H. Liu, J. Ge, Dyes Pigm. 65 (2005) 227–233.
[168] T.X.H. Le, R. Esmilaire, M. Drobek, M. Bechelany, C. Vallicari, D.L. Nguyen, A. Julbe, S. Tingry, M. Cretin, J. Mater. Chem. A 4 (2016) 17686–17693.
[169] H. Zhao, Y. Wang, Y. Wang, T. Cao, G. Zhao, Appl. Catal. B 125 (2012) 120–127.
[170] Tech Briefs, Electrochemical Hydrogen Peroxide Generator. https://www.techbriefs.com/component/content/article/tb/pub/techbriefs/manufacturing-prototyping/8625, 2010 (accessed 29 September 2021).
[171] HPNow, On-site Generation of Hydrogen Peroxide. https://www.hpnow.eu/, 2019 (accessed 29 September 2021).
[172] B. Puértolas, A.K. Hill, T. García, B. Solsona, L. Torrente-Murciano, Catal. Today 248 (2015) 115–127.
[173] C. Tang, Y. Zheng, M. Jaroniec, S.-Z. Qiao, Angew. Chem. Int. Ed. 60 (2021) 19572–19590.
[174] V.L. Kornienko, G.A. Kolyagin, G.V. Kornienko, N.V. Chaenko, A.M. Kosheleva, T.A. Kenova, I.S. Vasil'eva, Russ. J. Appl. Chem. 87 (2014) 1–15.
[175] N.V. Chaenko, G.V. Kornienko, V.L. Kornienko, Russ. J. Electrochem. 47 (2011) 230–233.
[176] Y.-L. Chen, T.-C. Chou, J. Appl. Electrochem. 26 (1996) 543–545.
[177] Y. Shen, M. Atobe, W. Li, T. Nonaka, Electrochim. Acta 48 (2003) 1041–1046.
[178] Q. Li, Y. Ouyang, S. Lu, X. Bai, Y. Zhang, L. Shi, C. Ling, J. Wang, Chem. Commun. 56 (2020) 9937–9949.
[179] F. Libisch, C. Huang, E.A. Carter, Acc. Chem. Res. 47 (2014) 2768–2775.
[180] Y. Wang, H.-P. Cheng, J. Phys. Chem. C 117 (2013) 2106–2112.
[181] L. Grajciar, C.J. Heard, A.A. Bondarenko, M.V. Polynski, J. Meeprasert, E.A. Pidko, P. Nachtigall, Chem. Soc. Rev. 47 (2018) 8307–8348.
[182] M. Zhong, K. Tran, Y. Min, C. Wang, Z. Wang, C.-T. Dinh, P. De Luna, Z. Yu, A.S. Rasouli, P. Brodersen, S. Sun, O. Voznyy, C.-S. Tan, M. Askerka, F. Che, M. Liu, A. Seifitokaldani, Y. Pang, S.-C. Lo, A. Ip, Z. Ulissi, E.H. Sargent, Nature 581 (2020) 178–183.
[183] L. Ge, H. Yuan, Y. Min, L. Li, S. Chen, L. Xu, W.A. Goddard III, J. Phys. Chem. Lett. 11 (2020) 869–876.
[184] M. Ruck, B. Garlyyev, F. Mayr, A.S. Bandarenka, A. Gagliardi, J. Phys. Chem. Lett. 11 (2020) 1773–1780.
[185] S. Lee, W. Jang, M. Kim, J.E. Shin, H.B. Park, N. Jung, D. Whang, Small 15 (2019) 1903705.